Journal of Volcanology and Geothermal Research 299 (2015) 103–129

Contents lists available at ScienceDirect

Journal of Volcanology and Geothermal Research

journal homepage: www.elsevier.com/locate/jvolgeores

The frequency and magnitude of post-glacial explosive eruptions at Volcán Mocho-Choshuenco, southern Chile

Harriet Rawson [a,*], José A. Naranjo [b], Victoria C. Smith [c], Karen Fontijn [a,d], David M. Pyle [a], Tamsin A. Mather [a], Hugo Moreno [e]

[a] Dept. Earth Sciences, University of Oxford, South Parks Road, Oxford OX1 3AN, UK
[b] Servicio Nacional de Geología y Minería, Avenida Santa María 0104, Santiago, Chile
[c] Research Lab. for Archaeology, University of Oxford, South Parks Road, Oxford OX1 3QY, UK
[d] Dept. Geology and Soil Science, Ghent University, Krijgslaan 281-S8, 9000 Gent, Belgium
[e] Observatorio Volcanológico de Los Andes del Sur, Servicio Nacional de Geología y Minería; Dinamarca 691, Temuco, Chile

ARTICLE INFO

Article history:
Received 20 November 2014
Accepted 16 April 2015
Available online 25 April 2015

Keywords:
Tephrochronology
Mocho-Choshuenco Volcano
Southern Volcanic Zone
Fe–Ti oxides
Plinian eruptions
Tephra
Glass chemistry

ABSTRACT

Volcán Mocho-Choshuenco (39°55′S 72°2′W) is one of the most hazardous volcanoes in Chile's Southern Volcanic Zone (SVZ). To better evaluate these hazards, we have reconstructed a high resolution eruption history, the most detailed to date for a volcano in Chile, from detailed field observations and geochemical analyses. Mocho-Choshuenco has experienced ca. 75 post-glacial (<18 ka) explosive eruptions, including three large (volume ≥1 km^3) Plinian eruptions (Neltume, Pirehueico and Huilo) and a large pyroclastic density current and associated sub-Plinian event (Enco). Poor preservation and lack of exposure made it difficult to distinguish between medial to distal deposits solely on field observations. Instead, deposits have been correlated using a combination of glass chemistry and Fe–Ti oxide compositions. New radiocarbon dates were obtained and integrated with existing dates in a Bayesian age model (OxCal) to constrain the tempo of the volcanism. Based on preserved deposits, we derive a post-glacial eruptive frequency of one explosive eruption every ~220 years with the youngest, confirmed eruption from Mocho-Choshuenco in 1864. The total post-glacial volume of tephra erupted is estimated at ≥20 km^3 (ca. 50% with a dacitic or rhyolitic glass composition) with ≥4 km^3 erupted from the monogenetic cones on the flanks, making Mocho-Choshuenco one of the most productive (ca. 1 km^3/kyr) and active volcanoes in the SVZ during post-glacial times. Many tephra deposits from Mocho-Choshuenco could be preserved in one or more lakes in the region, and have the potential to form regional tephra markers. In particular the Neltume deposits, which are dispersed to the NNE, are found interbedded with tephra deposits from the Villarrica–Quetrupillán–Lanín chain and should be preserved around Sollipulli and Llaima (~140 km NNE of Mocho-Choshuenco). This study highlights how a multi-technique approach enables a complicated tephrostratigraphy to be unravelled so more robust estimates of the past eruptive frequency and size can be determined.

1. Introduction

Active volcanoes pose a significant natural hazard, and in order to evaluate the likelihoods of future scenarios it is necessary to understand the frequency, scale and impact of past eruptions. In particular, there is a pressing need to better understand the products of medium to large magnitude explosive events. This requires detailed work in both proximal and distal localities to construct the stratigraphic framework of significant events. Identifying and correlating the deposits of explosive eruptions is also important to enable their potential use as regional chronostratigraphic markers in palaeoenvironmental records (e.g., Naranjo and Stern, 1998; Watt et al., 2013a; Fontijn et al., 2014).

Tephra deposits are commonly poorly preserved, or exposed. This is most problematic in temperate and humid climates where weathering rates are high, such as southern Chile (e.g., Fontijn et al., 2014); or in very arid regions, such as northern Chile or eastern Patagonia, where the lack of vegetation enables tephra to be easily eroded (e.g., Fontijn et al., 2014). Poor preservation and lack of exposure can make it difficult to distinguish between the medial to distal deposits of eruptions of magmas of similar composition solely on field observations. Scarcity of outcrops is also problematic at volcanoes with a complex tephrostratigraphy as a result of high eruptive frequencies, such as at Mocho-Choshuenco. Microanalysis of glass and mineral components provides a tool to fingerprint these deposits as the products of different eruptions typically have distinct glass and/or mineral

* Corresponding author at: Dept. Earth Sciences, University of Oxford.
E-mail addresses: harrietrawson@gmail.com, harriet.rawson@earth.ox.ac.uk (H. Rawson).

http://dx.doi.org/10.1016/j.jvolgeores.2015.04.003

compositions (e.g., Fierstein, 2007; Lowe, 2011; Smith et al., 2011a), and only small amounts of sample are needed for analysis.

In southern Chile most prior work has relied on field observations (relative stratigraphic position of identified layers, their physical measurements and mapping their geometry) and limited whole-rock geochemical data to correlate tephra deposits (e.g., Stern, 1991). As whole-rock chemistry may vary with distance from the vent (as crystal content decreases with distance from the vent), is susceptible to the effects of weathering and tends not to vary much between units it is not a very robust technique for correlating tephra deposits. Increasingly tephra studies use the analysis of glass shards to fingerprint and correlate deposits (e.g., see Lowe, 2011 for a review). In southern Chile, the high weathering rates and rapid degradation of pumice samples pose a significant challenge to the use of glass for chemical correlation.

Mineral chemistry is another less commonly used tool for correlating tephra. Biotite, hornblende, pyroxenes and Fe–Ti oxides have all previously been used for tephra correlation (e.g., Lowe, 1988; Froggatt and Rogers, 1990; Shane, 1998; Shane, 2000; Shane et al., 2003; Fierstein, 2007; Smith et al., 2011a). The Fe–Ti oxides offer an excellent and underexploited potential for use as a discriminant between the deposits of different eruptions. Fe–Ti oxides are almost ubiquitous in tephra samples, they equilibrate rapidly with the melt (e.g., Bacon and Hirschmann, 1988; Venezky and Rutherford, 1999; Devine et al., 2003) and their compositions are sensitive to magmatic conditions, such as temperature and oxygen fugacity (Carmichael and Nicholls, 1967; Ghiorso and Evans, 2008). As a result, Fe–Ti oxides can be sensitive tracers of individual eruptive events (e.g., Shane, 1998; Fierstein, 2007; Marcaida et al., 2014).

Volcán Mocho-Choshuenco is a large compound stratovolcano in the Southern Volcanic Zone (SVZ) of Chile (Fig. 1). It lies in a region which is popular with tourists and close to several major population centres (over 400,000 people live within 100 km of the volcano), and presents a moderate level of volcanic hazard to the region. Nonetheless, the eruptive history of Mocho-Choshuenco is still poorly known, though it is clear that it that has experienced multiple large explosive eruptions during the Holocene whose timing and size remain poorly constrained (Moreno and Naranjo, 2006; Moreno and Lara, 2007; Fontijn et al., 2014). In this study we use field observations and major element chemistry of glass and Fe–Ti oxides to correlate the deposits of explosive eruptions from Mocho-Choshuenco between different locations in the region. This enables us to confidently correlate numerous deposits, despite variable preservation and distance from the eruptive source. This multi-technique approach also enables us to recognise many units for the first time, including a Plinian eruption (Huilo, MC9). Consequently the new event stratigraphy includes more eruptive units, and more quantitative details on the ages and sizes of past eruptions, than prior work. Our new high resolution stratigraphy of post-glacial explosive eruptions allows us to better constrain the past explosive activity, and reveals Mocho-Choshuenco to be one of the most productive and active volcanoes, in terms of explosivity, in the SVZ of Chile.

We present the work in three main sections; field stratigraphy (Section 3), tephra correlations (Section 4) and eruption size (Section 5). Section 3 focuses on the physical characteristics of the deposits, dispersal and their relative stratigraphic positions. Section 4 presents the geochemical data used to chemically fingerprint and correlate deposits, along with new radiocarbon dates and an age model to constrain eruption ages. Finally, in Section 5 we use these correlations to estimate the size of the eruptions. Although separate, all three sections are intrinsically linked; for example, units described in Section 3 could not have been identified without the chemical analyses presented in Section 4.

2. Geological setting

Mocho-Choshuenco is a late Quaternary volcanic complex located at 39°55′S 72°02′W in the SVZ (33°–46°S; Fig. 1) of southern Chile. It lies between Volcán Villarrica, 55 km to the north, and the Puyehue-Cordón Caulle volcanic complex, 70 km to the south. Mocho-Choshuenco is a glacially-capped complex that is interpreted as a compound volcano: Volcán Mocho has a 4 km wide caldera, infilled by a glacier, with a young scoria cone in the centre, called Mocho; Volcán Choshuenco, which forms part of the north-western rim of the caldera, has only been partially affected by the collapse so retains its conical form. Additionally there are circa (ca.) 40 minor scoria cones on the flanks (Moreno and Lara, 2007). The cones are subdivided into three groups: Fui (ca. 25 cones to the north-east and east of the edifice), Caunahue (ca. 10 cones on the south-west flank), and Ranquil (four cones on the north-east flank; Fig. 1). During the Llanquihue glaciation, the last glacial period in southern Chile, Mocho-Choshuenco would have been extensively glaciated until ca. 18 ka, when deglaciation began at these latitudes (Hulton et al., 2002; Glasser et al., 2008; Kaplan et al., 2008).

2.1. Previous work

Moreno and Lara (2007) grouped the volcanic deposits from the Mocho-Choshuenco edifice into eight units, classified by age and source. Deposits from the Volcán Choshuenco peak are labelled Unidad Choshuenco (UC) and those from Volcán Mocho are labelled Unidad Mocho (UM). Additionally units are grouped by age from oldest UM1 to youngest UM5 (illustrated in Table 2). The eighth unit, Secuencia Piroclástica, comprises all the deposits from explosive eruptions preserved within the other seven units. As glaciers often erode down to the 'bedrock', the only tephra deposits that are widely preserved in proximal and medial locations are those that post-date the most recent deglaciation (i.e., UM4 and UM5). This study focuses on these post-glacial tephra deposits. The base of unit UM4 is placed at ca. 18 ka, the present estimate of when deglaciation began (e.g., Watt et al., 2013b). The boundary between UM4 and UM5 is marked by an eruption called 'Enco' and is placed at ca. 1.7–1.5 cal. ka BP using newly calibrated and modelled radiocarbon ages (see Section 4.2.2).

In their previous work, Moreno and Lara (2007) presented evidence for three large post-glacial eruptions. Two formed widespread dacitic pumice fall deposits, Neltume and Pirehueico (Table 1), which are named after the village closest to the edifice that lies on the dispersal axis. The Neltume deposits are considered to be the oldest and largest preserved Plinian fall deposits from Mocho-Choshuenco and were first described by Echegaray et al. (1994). The Pirehueico deposits are the products of another major Plinian eruption, first identified by Pérez (2005) and are considered to be the second oldest and second largest preserved Plinian fall deposits from Mocho-Choshuenco. The third is a scoria fall deposit overlain by a pyroclastic density current (PDC; interpreted in previous studies as an ignimbrite), which is called Enco after the village where the thickest PDC deposits are found (Moreno and Lara, 2007; Table 2). This unit is the youngest of the three major eruptions. Further, possible historic events are summarised in Table 2 including 1864, the youngest confirmed eruption from Mocho-Choshuenco. Our work draws on seven field seasons at Mocho-Choshuenco between 1998 and 2014, focusing on the post-glacial tephra deposits. This work reveals the presence of many previously undescribed tephra deposits and expands our knowledge of the late Quaternary eruption record of this major volcanic centre.

3. Field stratigraphy

Late Quaternary tephra deposits from Mocho-Choshuenco are found in scattered exposures around the edifice as far north as Volcán Quetrupillán (ca. 70 km) and as far east as San Martín de Los Andes (ca. 65 km; Fig. 1). Approximately 400 localities were visited during fieldwork. Outcrops at these localities were predominantly road-cuttings where tephra layers were preserved either bounded by well-developed palaeosols or draped over glacially eroded basement or the post-glacial scoria cones that also form part of the Mocho-Choshuenco Complex. Outcrop exposure varies considerably in scale (1–20 m), as

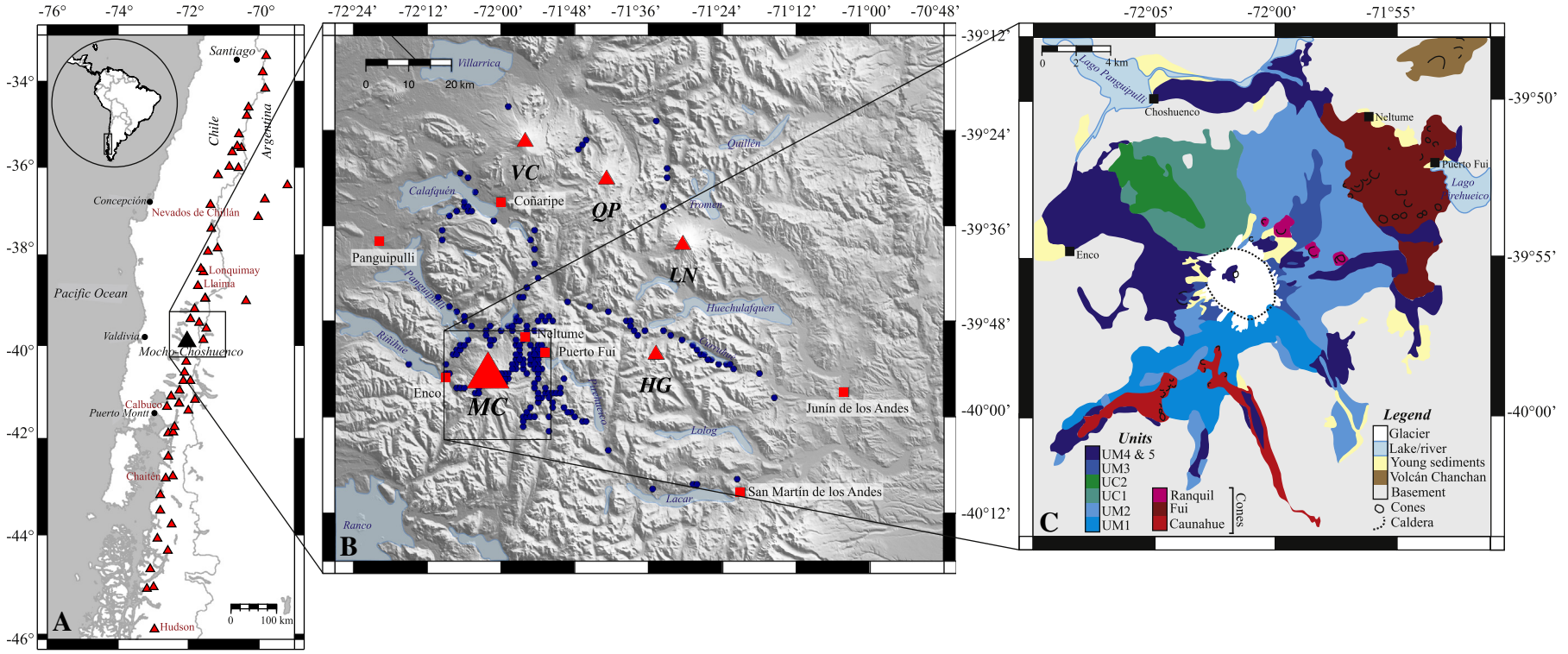

Fig. 1. A: Map of the Southern Volcanic Zone (SVZ). Volcanoes that have been active in the Holocene are marked with red triangles. Mocho-Choshuenco is marked by the black triangle. B: The region around Mocho-Choshuenco (MC). Localities where deposits from MC are found are marked with a dark-blue circle, other volcanoes are marked with a red triangle (Villarrica (VC), Quetrupillán (QP), Lanín (LN), Huanquihue Group (HG)) and towns are labelled and marked with a red square. C: Simplified geological map adapted from Moreno and Lara (2007). Units are labelled as in Table 1. (For interpretation of the references to colour in this figure legend, the reader is referred to the web version of this article.)

Table 1
Stratigraphic summary and proposed nomenclature of the volcanic deposits from Mocho-Choshuenco.

	Units	Sub-units	Category
Unidad Mocho 5	MC25 (Riñihue)		β
(ca. 1.7 cal. ka BP-present)	MC24		γ
	MC23 (Arauco)		β
	MC22		γ
	MC21 (Pilmaiquén)		β
	MC20	MC20B	β
		MC20A	
	MC19		γ
	MC18 (Hua-hum)	MC18C	α
		MC18B	
		MC18A	
	MC17		γ
	MC16		γ
Unidad Mocho 4	MC15 (Enco)	MC15E	α
(ca. 18–1.7 cal. ka BP)		MC15D	
		MC15C	
		MC15B	
		MC15A	
	MC14		γ
	MC13		β
	MC12		β
	MC11		γ
	MC10 (Grupo Fui Tephra)	MC10H	α
		MC10G	
		MC10F	
		MC10E	
		MC10D	
		MC10C	
		MC10B	
		MC10A	
	MC9 (Huilo)	MC9B	α
		MC9A	
	MC8		β
	MC7		γ
	MC6		γ
	MC5 (Pirehueico)	MC5F	α
		MC5E	
		MC5D	
		MC5C	
		MC5B	
		MC5A	
	MC4 (Neltume)	MC4C	α
		MC4B	
		MC4A	
	MC3		β
	MC2		γ
	MC1		γ
Unidad Choshuenco 2 (ca. 80–20 ka)			
Unidad Mocho 3 (ca. >60 ka)			
Unidad Choshuenco 1 (ca. >100 ka)			
Unidad Mocho 2 (ca. <200–130 ka)			
Unidad Mocho 1 (ca. >350–200 ka)			

The seven formations are taken from Moreno and Lara (2007). Units, and sub-units, are ordered by stratigraphic position with the oldest at the base. Units are given a name from MC1 (oldest) to MC25 (youngest); MC26 and MC27 have poor stratigraphic constraint so are not included. Some units have an additional name (given in brackets). The units are assigned to a category: Category α, Category β, and Category γ depending on their distribution and preservation (see text for more details). Age estimates for the formations are given in brackets. All, apart from Unidad Mocho 4 and 5 (UM4 and UM5), are the values given in Moreno and Lara (2007). UM4 and UM5, the focus of this study, include updated ages from newly calibrated and modelled radiocarbon ages within this study.

does unit thickness (from <5 cm to 8 m) and soil thickness (from a few cm to 60 cm). Dense vegetation, temperate climate and high annual rainfall contribute to the often poor exposure and preservation, making stratigraphic markers difficult to distinguish; even deposits from reasonably large explosive events (VEI ~ 4) may only be preserved in very few localities (e.g., MC3, 3 localities). The best exposures were found in road-cuttings. However, few localities preserve multiple tephra units, and there is no known outcrop that preserves the complete stratigraphy. Many localities visited in early field seasons (by JAN and HM) no longer exist or are no longer accessible due to changes in the road network.

Field work in proximal locations revealed tephra deposits from numerous eruptions. Each tephra deposit bounded by a palaeosol is attributed to a separate eruption, however we acknowledge that there may be insufficient time between two eruptions for soils to develop. Hence what we interpret as a 'single eruption' could still represent multiple events, or events sustained over an extended period of time. This has potential consequences for the predicted frequency, intensity and scale of explosive eruptions. We describe deposits from 34 explosive eruptions in the post-glacial succession. These we assign to 27 eruptive units, which we label from oldest (MC1) to youngest (MC25; relative stratigraphic position illustrated in Table 1). Additionally we categorise these 27 units by their relative distribution and preservation. Units widely distributed and well preserved are assigned to Category 'α', those moderately distributed and preserved to Category 'β' and finally those that have limited distribution and poorly preservation to Category 'γ'. As there is an inherent bias in the rock record these categories do not always directly correlate to eruption size. For example, older deposits have a greater likelihood of being deeply buried and hence require deeper road cuts to be exposed. Therefore older units are not always exposed at the surface and hence may appear poorly distributed and preserved relative to younger units formed by eruptions of comparable size. Equally, the products of eruptions with narrow or uni-directional dispersal axes may be undersampled, compared to the products of eruptions of equivalent size that had a more even distribution.

Of the 27 eruption units identified we confirm the recognition of the previously identified pumice fall deposits of Neltume (MC4) and Pirehueico (MC5) and the large scoria fall and PDC unit of Enco (MC15). In addition to these 27 units, we identify numerous scoria fall deposits interbedded with the pumice fall deposits and palaeosols. These typically are nondescript, black-red, well sorted, fine-medium lapilli scoria fall deposits with microlite-rich glass and rare Fe–Ti oxides, which are rarely possible to chemically fingerprint and correlate. Most of these scoria deposits are likely to record small Strombolian eruptions originating from one of the many scoria cones that can be found on the flanks of Mocho-Choshuenco (ca. 40 cones). However, unless there are associated lava flows (e.g., column I, Fig. 2) or the clasts are very large and clearly have a proximal origin (e.g., column K, Fig. 2) it is not possible to confidently assign the origin of most deposits to a specific scoria cone or to the main edifice (central vent). To avoid duplication, these deposits were only labelled if they could be chemically fingerprinted (e.g., MC1). Consequently only 34 of the ca. 75 post-glacial eruptions are described and assigned a unit name. Furthermore since the palaeoenvironments are highly variable, it has not yet proved possible to correlate palaeosols, and we make no attempt to formalise their stratigraphy.

3.1. Field sampling

Samples and measurements were taken of the tephra deposits preserved in both proximal and distal locations. Measurements of deposit thickness and maximum clast size of pumice, scoria, lithics and, if present, ballistic bombs, were made where possible. Any evidence of slumping, avalanche bedding, fragmented clasts and bombs was noted and taken into account when constructing the isopach and isopleth maps (see Section 5). Maximum clast size was determined from the geometric mean of the three axes of each of the five largest clasts at an outcrop. The geometric mean of these five measurements gives the maximum clast estimate. In early field seasons (1998 to 2006), we determined maximum clast size by measuring only the maximum diameter of the five largest, most spherical clasts. This difference in method is taken into account when drawing isopleth maps of maximum clast size.

Table 2
Summary of previous knowledge of the post-glacial explosive history of Mocho-Choshuenco.

Eruption name	Other names in literature	Description	Dispersal	Volume (km^3)	VEI	Date/Age (uncalibrated yrs)	Reference
MC25 (Riñihue)	1864, FP4	Pyroclastic flows, surges, lahars	SW		2	1–3 (±1 day) November 1864 AD	1, 2, 3
1822		Possible small historic eruption			2	1822 AD	3
1777		Possible small historic eruption			2	1777 AD	3
1759		Possible small historic eruption			2	1759 AD	3
MC15 (Enco)	FPPJB, OPFUY, OPL, FP3	Ignimbrite and scoria fall	Radial			1700 BP	1, 4, 5
MC5 (Pirehueico)	Pp2	Andesitic pumice fall	E and NE	~1		8200–6700 BP	1, 4
MC4 (Neltume)	PpCh1, PpN	Dacitic pumice fall	NNE	2.5–2.9	5	10,700–9700 BP	1, 4, 5, 6
Previous names for Volcán Mocho-Choshuenco	Valdivia, Rauco, Lajara, Penguipulli, Panguipulli, Riñihue, Quetrupillan, Renihue, Shoshuenco						3

Volcanic Explosivity Index (VEI) devised by Newhall and Self (1982). References: [1] Moreno and Lara (2007), [2] Vidal Gormaz (1869), [3] Sepulveda (2004), [4] Pérez (2005), [5] Echegaray (2004), [6] Echegaray et al. (1994).

However, it is unlikely to be significant compared to the effects of post-depositional compaction and weathering.

Bulk samples of tephra and samples of individual pumice, scoria or lithic clasts were taken at ca. 175 sites, providing a set of more than 275 samples. Preliminary correlations in the field were made based on stratigraphic position and physical characteristics such as colour, lithic abundance, lithic type and grain size.

3.2. Field descriptions

We identify 27 volcanic deposits that are described below and in Table 3. We interpret each unit to be the products of a separate explosive eruption. Sub-units are labelled with a letter after the name (e.g., MC15A). Within the text we describe the units assigned to preservation categories α, β and γ, as defined in Table 1. Within each category we describe the units from oldest to youngest. Deposit and clast descriptions, type localities and deposit interpretations are described in Table 3. Key field photos (Fig. 3) and SEM images of typical glass shards (Fig. 4) are also included for units in categories α and β. The notation of maximum pumice (MP), maximum scoria (MS) and maximum lithic (ML) is used. Key localities, not illustrated in Fig. 2, are presented in the text with their locality name (e.g., 120114-13) and GPS co-ordinates (latitude, longitude; WGS84 datum). All distances (km) from summit are measured from the centre of the Mocho scoria cone within the caldera of Mocho-Choshuenco.

3.2.1. Category α

These units are the most widely dispersed and preserved from the Mocho-Choshuenco Volcanic Complex. Typically deposits are found at more than 10 localities up to at least 15 km from the summit. Four pumice fall deposits, one scoria fall and PDC unit, and a scoria package are assigned to this category: MC4 (Neltume), MC5 (Pirehueico), MC9 (Huilo), MC10 (Grupo Fui Tephra), MC15 (Enco) and MC18 (Hua-Hum).

3.2.1.1. MC4 (Neltume Pumice). The Plinian-style Neltume eruption produced a major pumice fall deposit, dispersed to the NNE and normally found resting conformably on top of a well-developed palaeosol and/or glacially eroded basement (typically either the Jurassic Tonalite of the Plutón Panguipulli, or the Triassic metasediments of the Formación Panguipulli, Moreno and Lara, 2007). In some proximal localities Neltume Pumice deposits overlie pumice deposits of MC3 and/or minor scoria fall deposits (e.g., MC1) that likely originate from nearby scoria cones (e.g., columns A, C, Fig. 2).

Internally, MC4 is a tripartite unit (e.g., column B, Figs. 2, 3B): at its base is a fine grey ash, interpreted as a vent clearing event (MC4A); This is overlain by a minor, fine-lapilli sized, orange-weathered pumice deposit (MC4B); and capped by the main sub-unit, an orange-weathered, well-sorted, lithic-poor pumice deposit (MC4C). In distal localities (when total thickness ca. <15 cm) the main sub-unit appears zoned as a result of variations in componentry (Fig. 3D). This is clearly seen at 030114-4 (39°30′S 71°33′W; MP of 0.4 cm and thickness of 11 cm) where the bottom two thirds (bottom 7 cm; Fig. 3D) weathers orange, as in more proximal localities, and changes sharply to dark-grey–yellow weathering in the upper third. This main unit, and underlying finer pumice unit, are interpreted as the deposits of a Plinian-style eruption as they are widely dispersed and thicknesses greater than 1 m are commonly preserved.

Deposits from the Neltume unit (MC4) are abundant and narrowly dispersed to the NNE. The thickest deposits of this unit are found NNE of the edifice, along the dispersal axis mid-way between the villages of Neltume and Choshuenco (Fig. 1). Here fallout deposit thicknesses (MC4C) reach 8 m and bombs up to 19 cm are preserved (e.g., 160114-1 at 39°50′S 72°3′W, 12 km from summit). The most continuous deposits are found along Ruta 203, along the eastern shore of Lago Panguipulli. The most distal localities with confirmed Neltume deposits are on the northern flank of Volcán Villarrica (63 cm thick, locality 030113-1 at 39°21′S 71°59′W, 65 km north of summit), near the town of Curarrehue (7 cm thick, 310100-3 at 39°21′S 71°36′W, 75 km NNE of summit) and on the northern flank of Volcán Lanín (27 cm thick, CLD163 at 39°34′S 71°32′W, 60 km north-east of summit).

The Neltume deposits are typically capped by a well-developed palaeosol that commonly includes reworked pumice clasts. This palaeosol separates the Neltume deposits from those of the overlying Pirehueico unit (MC5), described next.

3.2.1.2. MC5 (Pirehueico Pumice). The Plinian-style Pirehueico eruption produced a major pumice fall deposit that typically rests conformably on top of a well-developed soil and, in places, MC4 (Neltume) deposits (e.g., 130207-01 at 39°49′S 71°39′W). In a few outcrops, a thin (<2 cm) fine-lapilli scoria fall unit is found at the base of MC5, with no clear palaeosol horizon between (e.g., column F, Fig. 2).

The Pirehueico Pumice is the most complex of the large pumice units from Mocho-Choshuenco with 6 distinct beds preserved (e.g., column E, Fig. 2; Table 3; Fig. 3E–G). The deposits, dispersed to the east, are primarily orange weathered, well to moderately sorted, pumice-rich, with variable lithic and clast sizes between the sub-units. Two minor, grey-brown, fine-medium ash layers (MC5B and MC5E) are interbedded within the sequence. The deposits are interpreted as the result of a Plinian-style pumice fall with possible interbedded minor PDC deposits. Alternatively these fine ash layers (MC5B, E) could represent the time between eruption pulses, during which finer ash, from within the main fallout, was able to settle.

Deposits from this event are best preserved along the road parallel to the southern shore of Lago Curruhué, 30 km due west of Junín de los Andes, Argentina. The thickest fall deposits of Pirehueico Pumice are found east of the edifice, along the dispersal axis and within the Huilo-Huilo Biological Reserve. Here thicknesses up to 3 m and bombs up to 25 cm are preserved (e.g., 130117-06 at 39°56′S 71°50′W, 16 km east of summit). The most distal locality where Pirehueico

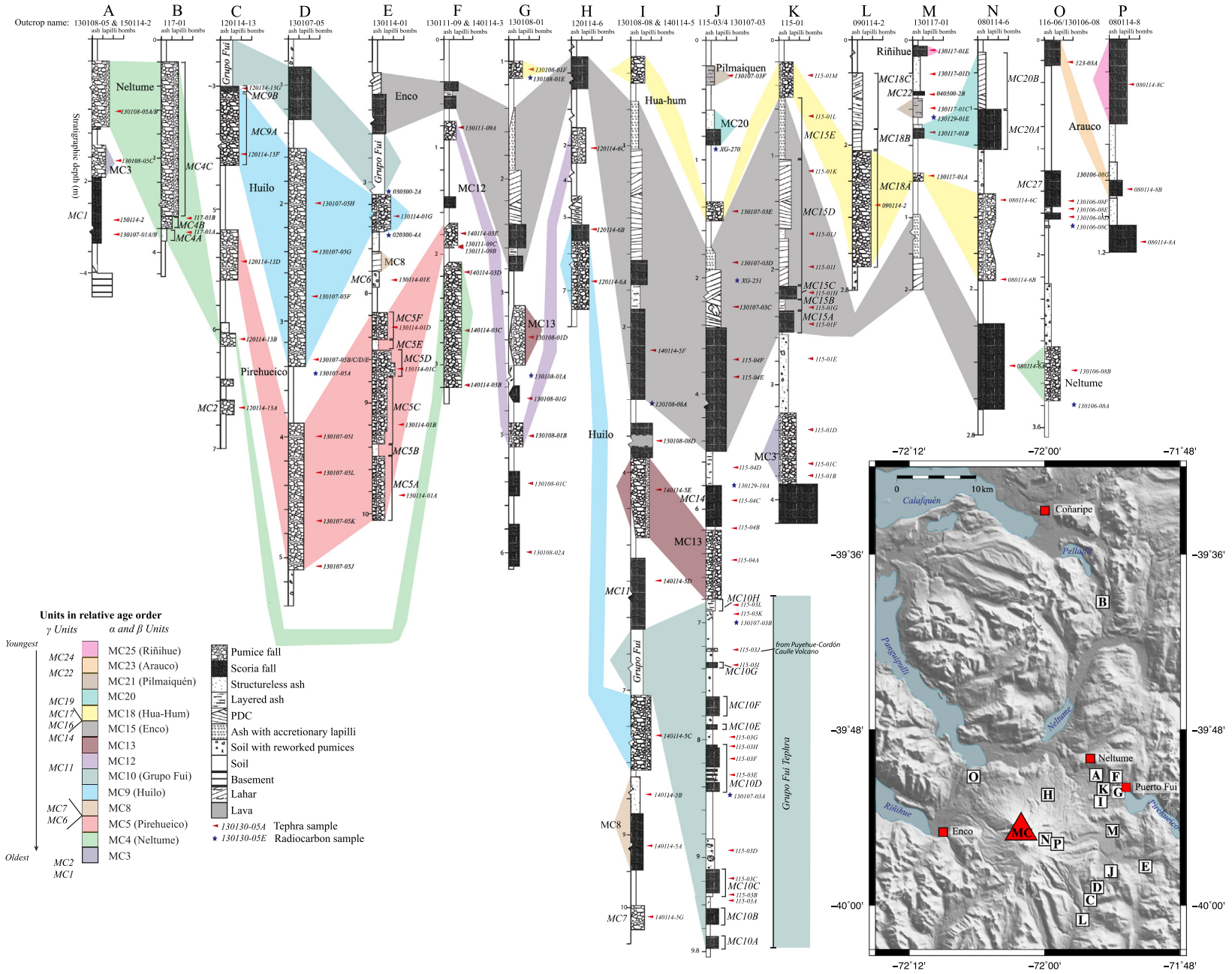

Fig. 2. Sixteen key localities that preserve Mocho-Choshuenco pyroclastic units. Locations of tephra (red triangles) and carbon (blue star) samples are marked. Correlations between sites are based on stratigraphic position and physical and chemical characteristics (glass and Fe–Ti oxide compositions) of the deposits. The units, and most sub-units, are labelled on the columns. Only units that comprise categories α and β are correlated between multiple localities and assigned a colour. All of these columns are labelled on the map, to the right. The vertical scale is in metres with a tick every 0.2 m. (For interpretation of the references to colour in this figure legend, the reader is referred to the web version of this article.)

deposits are confirmed is near Junín de Los Andes (27 cm thick, 170399-11 at 39°58′S 71°16′W, 66 km east of summit).

The Pirehueico deposits are capped by a well-developed palaeosol, commonly with pumice clasts and charcoal pieces. At one locality (column E, Fig. 2) there is a pumice-rich horizon within the palaeosol, which we interpret as a reworked pumice fall (MC6) based on geochemical data (see Section 4).

3.2.1.3. MC9 (Huilo Pumice). The Plinian-style Huilo eruption produced a major pumice fall deposit that typically rests conformably on top of a well-developed palaeosol and deposits from the Neltume (MC4) eruption (e.g., 130120-02, 39°49′S 71°58′W). At rare outcrops to the east it sits above, separated by a palaeosol, the Pirehueico (MC5) deposits (e.g., column D, Fig. 2) and the scoria fall and flow MC8 (e.g., 130131-03, 39°55′S 71°55′W; MC8 described in Section 3.2.2).

Internally two distinct beds are preserved. The main, lower bed (MC9A) is an orange-weathered, well-sorted, massive, lithic-poor (ca. <5%) pumice deposit (e.g., column D, Fig. 2), interpreted as the deposits of a Plinian-style eruption. At rare outcrops, where the thickest Huilo Pumice deposits are preserved, a second, upper bed (MC9B) is visible (e.g., column C, Fig. 2). Here the pumice deposit has a sharp upper contact (i.e., no gradation between beds) with a thin continuous scoria layer (Fig. 3G, H) resting conformably on top. This layer is often <10 cm thick and oxidised red. Its limited preservation and presence only to the east of the edifice suggests that this scoria unit may originate from a nearby scoria cone, which erupted immediately after the Plinian-style eruption.

Deposits are relatively abundant and quite broadly dispersed to the east. The thickest fallout deposits (MC9A) are found east of the edifice, just south of the dispersal axis, which trends east, and within the Huilo-Huilo Biological Reserve. Here thicknesses up to 3.3 m are preserved (e.g., 100114-5 at 39°5′S 71°52′W, 15 km east of summit). The most distal locality where Huilo deposits are confirmed is near Lago Huechulafquen (20 cm thick, 130207-04 at 39°49′S 71°37′W, 38 km ENE of summit).

The Huilo deposits are overlain by a well-developed palaeosol commonly with reworked pumice clasts from MC9A. This palaeosol separates the Huilo deposits from those of the Grupo Fui Tephra package (MC10), described next. At one locality (column H, Fig. 2), immediately above the Huilo unit, a light-grey, 95 cm thick laminated succession of fines-depleted layers (each 1–10 cm thick), which are primarily planar bedded although some preserve cross bedding, is interpreted as a reworked ash deposit with some characteristic lahar features (e.g., matrix supported and sub-angular clasts; Fig. 3H).

3.2.1.4. MC10 (The Grupo Fui Tephra). The Grupo Fui Tephra comprises multiple coarse-ash to medium-lapilli sized, scoria and ash deposits separated by palaeosols (Fig. 3I–K); we define 8 sub-units in Table 3. Preservation of this unit is poor. Most of the scoria is moderately vesicular, weathers orange, and often has little to no fresh glass preserved. The deposits are predominantly preserved to the east and ENE of the main edifice in the area between the volcano and Lago Pirehueico (Fig. 1). This area is also where the greatest concentration of scoria cones is found, and it is inferred that the majority of these deposits, most of which are falls, originate from the cones, rather than from the main edifice. A poorly dispersed scoria unit (MC11; e.g., column I, Fig. 2) overlies the Grupo Fui Tephra deposits. This is bound by a palaeosol, which is overlain in turn by deposits from MC12 and MC13 (Section 3.2.2).

3.2.1.5. MC15 (Enco). The Enco eruption produced a sub-Plinian scoria fall and a major scoriaceous PDC unit. Deposits typically rest conformably on top of a well-developed palaeosol and, separated by the palaeosol, the deposits of Neltume (MC4), Huilo (MC9) or the Grupo Fui Tephra (MC10). The base of the Enco deposit is not exposed to the west (e.g., 130106-01 at 39°56′S 72°06′W), while few Enco deposits have been found to the south due to limited road access. Here, deposits typically infill the palaeotopography such that the base of the deposit is not exposed (e.g., 050300-2 at 40°0′S 72°7′W).

Internally five separate sub-units are preserved (detailed descriptions in Table 3): MC15A is a well sorted, black scoria fall, which rests conformably on top of a well-developed palaeosol; MC15B deposits comprise mm-scale, grey–black–yellow, parallel bands of ash, which have a diffuse, gradational basal contact with MC15A; MC15C is a moderately-well sorted, black scoria fall that rests conformably on top of MC15B; MC15D is a poorly sorted, cross-bedded, grey-weathered PDC deposit that sharply erodes MC15C; and finally MC15E is a grey, ash deposit containing ash pellets and rare accretionary lapilli, with a diffuse, gradational contact with MC15D.

A grey ash (MC15E) at the top of the Enco sequence typically grades into a well-developed palaeosol, which separates the Enco deposits from those of the overlying Hua-Hum event (MC18). At one outcrop (130106-03 at 39°56′S 72°06′W) the PDC deposits of MC15D are sharply eroded by another scoriaceous PDC deposit (MC26), which is thought to originate from the lateral collapse of the Tumba Buey Scoria cone, a large collapsed scoria cone on the western flank of Mocho-Choshuenco 3 km east of this locality. Substantial lahar deposits, with thicknesses <10 m, are also associated with the Enco units. These are principally found to the north-west, along the road between the villages of Enco and Choshuenco (e.g., 150114-11 at 39°53′S 72°09′W), and to the south, in Pampa-Pilmaiquén along the valley of the Pillanleufú River (e.g., 090114-3 at 40°1′S 71°57′W), where they clearly postdate the main PDC deposits of the Enco eruption. The lahar deposits are a succession of grey beds that can be divided into three main levels; the base (<2.5 m thick) is a fine-depleted, densely laminated deposit with scarce, sub-angular lithic fragments of lavas <20 cm; the middle deposit (<2 m thick) is characterised by abundant lava blocks (<50 cm) in a sandy matrix; and the top level reaches <6 m thick and contains imbricated blocks immersed in a predominantly sand-rich matrix that shows diffuse bedding. These deposits possibly represent the interstratification of lahar flood-plain, transition and lahar-runout facies (Scott, 1988).

The Enco deposits are widespread radially around the volcano. The thickest fall deposits are found east of the edifice, along the dispersal axis and mid-way between the edifice and Lago Pirehueico. Here thicknesses of 2.1 m and bombs of 13 cm are preserved (e.g., 130129-10 at 39°57′S 71°54′W, 11 km east of summit). The thickest PDC deposits are found to the west, near the Refugio Universidad Austral, with thicknesses up to 70 m and clasts up to 30 cm (e.g., 130106-01 at 39°56′S 72°06′W, 6 km west of summit). On the eastern flank, just above the tree line, bombs >1 m are preserved (e.g., 070114-8 at 39°55′S 71°59′W, 4.5 km east of summit).

3.2.1.6. MC18 (Hua-Hum). These pumice deposits typically sit conformably on top of a well-developed palaeosol and deposits from the Enco (MC15) eruption (e.g., column K, Fig. 2). To the north-east, where often they constitute the youngest unit preserved, MC18 deposits commonly grade into the overlying palaeosol. However, to the east between the summit and Lago Pirehueico, they normally sit beneath, separated by a palaeosol, deposits from MC20 and Pilmaiquén (MC21). The deposits, dispersed to the north-east and south-east, vary in thickness from 80 cm, 10.4 km south-east of the summit, to 15 cm, 23.8 km ESE and 48 cm thick at 6.7 km to 30 cm at 12.9 km to the north-east of the summit.

Internally unit MC18 comprises three sub-units (Fig. 3O): a basal orange-brown pumice deposit inferred to be a sub-Plinian fall deposit (MC18A); a grey, moderately sorted, fine-ash unit interpreted as a PDC (*surge*; MC18B) deposit; and a sub-rounded, lithic-rich and pumice-rich deposit with a vesicular ashy matrix that could be interpreted as a wet PDC deposit (MC18C). MC18B and MC18C (column L, Fig. 2) are only preserved at one locality; this is near the mouth of one of the deepest flank valleys to the south-east of the summit. The Hua-Hum deposits are overlain by a well-developed palaeosol. At rare localities, to the SSE, deposits are interbedded with deposits from Puyehue-Cordón Caulle (e.g., CLD153, 40°14′S 71°57′W).

Table 3
Field descriptions, interpretations and type localities for the post-glacial tephra deposits.

Unit		Field description		Interpretation	Type locality					Photo in Fig. 3	SEM in Fig. 4
Name	Subunits	Deposit appearance	Clasts		Column in Fig. 2		MP/MS (cm)	ML (cm)	Th (cm)		
MC25 (Riñihue)		Well-moderately-sorted, black, fine to coarse-lapilli size scoria deposit. On edifice bombs up to 20 cm are found.	Black, vesicular, iridescent, scoria	Scoria fall	P	39°56′S 72°0′W			47	T, U	Q
MC24		Black, fine-medium-lapilli sized scoria deposit	Black, vesicular scoria	Scoria fall		39°55′S 71°59′W					
MC23 (Arauco)		Well-sorted, ungraded, scoria deposit. On edifice bombs are preserved (<25 cm)	Medium-lapilli sized, vesicular, black, iridescent scoria	Scoria fall	O	39°51′S 72°6′W			25	T	P
MC22		Thin, well-sorted, dense, fine-lapilli scoria deposit	Black, dense, vesicular scoria.	Scoria fall	M	39°55′S 71°53′W					
MC21 (Pilmaiquén)		Indurated, cm-scale thickness, well-sorted, parallel bands comprising grey, medium-ash to fine-lapilli sized clasts. Coarser layers are more loosely consolidated, particularly the top layer, which is not always preserved. The well-sorted top layer weathers grey, is ca. 75% the total thickness of lower bands and comprises fine-lapilli-sized, scoria clasts. Deposits commonly drape over topography and have a roughly uniform thickness over distances of 10s of metres. Rare localities preserve cross-bedding.	Fine-lapilli sized, vesicular, black, scoria	Wet scoria fall. Bands may record pulsating. Flow-like features may be secondary and arise from reworking	100 m south of M	39°55′S 71°54′W	1.4		31	R, S	O
MC20	MC20B	Well-moderately-sorted, grey, fine ash to fine-lapilli sized deposits. Sorting is poorer in more proximal localities where cm-scale, low-angle, cross bedding structures are preserved.		PDC (*surge*)	N	39°54′S 71°58′W			30	P, Q, R	
	MC20A	Moderate-poorly-sorted yellow weathered scoria deposit. In proximal localities fine-coarse lapilli sized clasts with abundant bombs (up to 20 cm).	Yellow weathered, very vesicular, crystal poor, scoria clasts. Large clasts (>10 cm) retain their black appearance in the cores. In more distal localities the scoria appears less vesicular and has a pumice-like appearance.	Scoria fall			20 (bombs)		23	P, Q, R	N
MC19		Grey-brown ash with yellow weathered pumice clasts	Weathered, yellow, vesicular, crystal poor pumice clasts.	Pumice fall		39°53′S 71°58′W	1.1		5		
MC18 (Hua-Hum)	MC18C	Sub-rounded lithic-rich and pumice-rich deposit with a bubble-rich ashy matrix		PDC Only preserved at one locality	L	40°1′S 71°57′W			28	O	
	MC18B	Moderately-poorly-sorted, grey, coarse ash to fine-lapilli sized deposit		PDC (*surge*) Only preserved at one locality					13	O	
	MC18A	Well-sorted, ungraded, orange-brown weathered, lithic-poor, medium-lapilli sized pumice deposit.	Orange-brown weathered, very vesicular and crystal poor pumice. Lithics are rare (ca. <5%), black, angular, glassy, poorly vesicular clasts.	Subplinian pumice fall			7.1	3.6	40	O, Q, R	M
MC17		Moderately-well-sorted, dark-grey-brown, medium-lapilli sized scoria deposit. Comprises rare small bombs (up to 6 cm).	Grey-brown, vesicular scoria	Scoria fall		39°54′S 71°58′W			18		
MC16		Well-sorted, brown-black weathered, fine-lapilli sized scoria deposit	Brown-black, slightly vesicular scoria	Scoria fall		39°54′S 71°58′W			15		

MC15 (Enco)	MC15E	Normally graded, grey, medium-ash, rich, particularly near the contact with MC15D, in both coated ash pellets and, more rarely, accretionary lapilli (typically <2 cm). Top usually grades into a well-developed palaeosol.	Heterogeneous ash with no modal glass morphology and abundant xenoliths of country rock and glass shards of older tephra units.	PDC	K	39°52′S 71°55′W			<55		
	MC15D	Poorly-sorted, indurated, cross-bedded (low-angle, 10′s cm-scale), grey-weathered deposit with abundant lithics supported in a medium-coarse ash matrix. Separate flow packages distinguishable in proximal localities. Each package is typically 1–2 m thick and inversely graded. The base is a well-sorted cemented ash, 10–20 cm thick, with red–brown oxidised top and base. The top is marked by a scoria rich layer, or pinching lens, or a thin layer of black glassy clasts. Typically the lithic component decreases up the package.	Lithics are predominantly grey-black, pitted, sub-angular, lava clasts, red-orange hydrothermally altered clasts and chalky-weathered clasts of a felsic intrusive rock. Brown-weathered, medium lapilli sized, black, sub-rounded, vesicular scoria and fine lapilli sized, black, glassy clasts mark the top of the flow packages.	PDC (*ignimbrite*) with multiple different flow packages					110	M, N	
	MC15C	Moderately-well-sorted, black scoria deposit with a moderate amount of lithics and abundant bombs. No grading or shower-bedding preserved.	Medium-coarse-lapilli sized, black, vesicular, crystal poor, commonly iridescent scoria, which typically has a fresh appearance. Lithics (ca. 5–10%) are heterogeneous. Most are dense grey or black, angular glassy lava fragments or, more rarely, red-orange coloured (hydrothermal alteration), slightly iridescent, non-vesicular clasts.	Subplinian scoria fall			3		12	M	L
	MC15B	mm-scale grey, black and yellow, parallel bands of medium ash to fine lapilli.	Heterogeneous clasts with no modal glass morphology and abundant xenoliths of glass shards of older tephra units.	Recording pulsating plume activity					9	M	
	MC15A	Well-sorted, black scoria deposit with rare lithics. Inverse grading, in top fifth preserved only in proximal localities.	Medium-lapilli sized, black, crystal poor, angular, glassy scoria with small vesicles. Lithics (ca. 5%) are weathered, milky white, medium-grained, crystalline clasts, probably diorite.	Scoria fall			2		21	M	K
MC14		Orange-brown weathered, medium-lapilli sized, scoria deposit. Charcoal at base. In one locality cut by a minor, black, lava flow from a nearby cone.	Orange-brown weathered, black-brown, crystal poor, vesicular scoria	Scoria fall from nearby cone	G	39°52′S 71°53′W			100		
MC13		Moderately-well-sorted, massive, orange-white weathered, lithic-poor medium-lapilli sized pumice deposit.	Orange weathered, very vesicular, crystal poor pumice	Pumice fall	I	39°53′S 71°55′W	4.8	1.9	20–50	L	J
MC12		Well-sorted, ungraded, yellow-brown weathered, medium-fine-lapilli sized pumice deposit.	Clasts have a bimodal appearance. Both weather yellow-brown but one type is more angular, less vesicular, darker and typically smaller than the second pumice type, which has a more pumice, rather than scoria, appearance.	Pumice fall	G	39°52′S 71°53′W	1.3		20	L	I
MC11		Brown weathered, lithic-rich (particularly in bottom fifth), medium-lapilli sized scoria deposit	Black, very vesicular scoria	Scoria fall	I	39°53′S 71°55′W			100		

(continued on next page)

Table 3 (*continued*)

Unit		Field description		Interpretation	Type locality					Photo in Fig. 3	SEM in Fig. 4
Name	Subunits	Deposit appearance	Clasts		Column in Fig. 2		MP/MS (cm)	ML (cm)	Th (cm)		
MC10 (Grupo Fui Tephra)	MC10H	Well-sorted, indurated, dark-grey, coarse-ash with fine laminations, comprising slightly finer layers. Some oxidisation	Ash is heterogeneous in composition and microlite rich. Abundant xenoliths of country rock.	Wet ash fall	J	39°58′S 71°54′W			10	I, K	
	MC10G	Well-sorted, orange weathered, fine-lapilli sized, scoria deposit that grades into overlying palaeosol.	Same as MC10A	Scoria fall			<0.5		6		
	MC10F	Moderately-well-sorted, orange-weathered, medium-lapilli sized deposit	Same as MC10A	Scoria fall			1		15		
	MC10E	Well sorted, orange weathered, medium-lapilli sized scoria deposit	Same as MC10A	Scoria fall			0.5		4		
	MC10D	Banded, cm-scale thickness, well-sorted, grey-orange-yellow weathered, medium-ash to medium-lapilli sized ash and scoria deposit.	Same as MC10A	Scoria and ash falls			1.5		45	I, J, K	G
	MC10C	Indurated, dark-grey coarse-ash, overlain by a well sorted, orange-weathered, lithic-poor, medium-lapilli sized scoria deposit.	Same as MC10A	Scoria fall			2.4		25		H
	MC10B	Well-sorted, orange weathered, fine-lapilli sized, scoria deposit	Same as MC10A	Scoria fall					10		
	MC10A	Well-sorted, orange weathered, fine-lapilli sized, scoria deposit	Orange-yellow weathered, vesicular scoria. Very weathered with little to no glass preserved that has not altered to clay.	Scoria fall					15	I, K	
MC9 (Huilo)	MC9B	Thin, continuous, black, medium-lapilli sized, scoria deposit that is often oxidised. Sharply cuts MC9A.	Black, vesicular scoria	Scoria fall	C	40°00′S 71°56′W	4.5		10	G, H	F
	MC9A	Well-sorted, massive, orange-white weathered, lithic-poor pumice deposit.	Orange weathered, very vesicular, crystal poor pumice with red-pink cores. At rare localities they retain original white appearance. Minor amounts of both grey and banded, vesicular, crystal poor pumice (ca. <5%) of a similar size to the dominant white pumice. Lithics are black-grey, sub-rounded, slightly-vesicular dense clasts (ca. < 5%) and dense, grey, angular lava fragments (ca. <5%).	Plinian-style pumice fall			7.5		166	F, G, H, K	E
MC8		Moderately-sorted, black-red weathered, coarse-ash to fine-lapilli sized scoria rich deposit. Some localities preserve cross-bedding. In the thickest deposits shower-bedding is preserved.	Black-red, weathered, vesicular scoria	Scoria fall and PDC from nearby cone		39°55′S 71°55′W			>100	F	D
MC7		Moderately-well-sorted, brown weathered, coarse-ash to fine-lapilli sized pumice deposit	Brown weathered, crystal poor, vesicular pumice	Pumice fall	I	39°53′S 71°55′W			13		
MC6		Moderately-sorted, orange weathered, medium-lapilli sized pumice held in a fine-ash sized, brown-grey matrix with charcoal.	Yellow-pink weathered, crystal poor, vesicular pumice.	Palaeosol with reworked clasts from a potenital pumice fall	E	39°57′S 71°52′W	2.8		12	F	
MC5 (Pirehueico)	MC5F	Moderately-sorted, orange-weathered, fine-coarse-lapilli sized pumice deposit.	Same as MC5D	Plinian-style pumice fall with possible interbedded minor PDCs (*surges*?; i.e. MC5B and MC5E)	E	39°57′S 71°52′W	5		18	F, G	
	MC5E	Grey-brown, medium-fine ash layer containing a moderate amount of, possibly reworked, pumice clasts. Sharp contact with MC3D and MC3F	Yellow-weathered, crystal poor, vesicular pumice.						9	F	
	MC5D	Moderately-well-sorted, orange-red weathered, moderate lithics, medium-lapilli to bomb-size pumice deposit. High concentration of bombs (up to 25 cm), particularly in bottom 75% of the deposit. Sharp contact with MC3C and MC3E.	Same as MC5A.				>7.5 (bombs <25 cm)	4.5	80	F	

	MC5C	Well-sorted, yellow-weathered, lithic-rich, fine-medium-lapilli sized, pumice deposit. The base is slightly finer; fine-lapilli sized clasts.	Same as MC5A			4		62	E		C
	MC5B	Fine, grey ash with no internal structures. Sharp contact with MC5A and MC5B.	Very weathered, heterogeneous ash, with glass having a devitrified appearance on the edges where it has altered to clay.					10	E		
	MC5A	Moderately-sorted, yellow-weathered, coarse-ash to medium-lapilli sized pumice deposit. Pumice are set in a lithic-rich (ca. 30%) and grey, ash-rich matrix.	Yellow-weathered, crystal poor, vesicular pumice, some with a mingled appearance. Lithics are predominately black-grey, angular, glassy, non-vesicular clasts and minor amounts of black-grey scoria.			3.3		60	E		
MC4 (Neltume)	MC4C	Well-sorted, orange-yellow-weathered, lithic-poor pumice deposit. Normal grading in the upper quarter observed at rare localities. Typically at distal localities (when thickness ca. <15 cm) the bottom two-thirds, of the deposit, weathers orange, as in more proximal localities, and this sharply changes to dark-grey-yellow weathering in the upper part.	Primarily, orange-yellow weathered, crystal poor, vesicular pumice with, at rare localities, white cores. Moderate amounts (ca. 5%) of grey and banded vesicular, crystal poor pumice and dense cauliform-shaped clasts (<5%) are uniformly distributed through the deposit and more abundantly preserved in proximal localities. Some proximal pumice preserve tuffsite veins and cauliform shaped black clasts trapped within vesicles.	Plinian-style pumice fall	B	39°39′S 71°55′W	2.5	0.7	300	B, C, D	B	
	MC4B	Very-well sorted, orange-yellow weathered, lithic-poor, fine-lapilli sized, pumice deposit that is typically <15 cm.	Fine-lapilli sized, orange-yellow-weathered, vesicular, pumice that only have small patches of glass not altered to clay	Pumice fall		0.7		10	B		
	MC4A	Well-sorted, grey, fine ash bounded by red-brown oxidised layers and typically <10 cm	Ash is heterogeneous in composition and only small patches of glass not altered to clay. Abundant xenoliths of country rock and glass shards of older tephra units.	Phreatomagmatic, vent-clearing event		fine ash		9	B		
MC3		Well-sorted, orange-yellow weathered, fine-medium-lapilli sized, pumice deposit. Lithic content changes sharply from ca. 40%, in the bottom half of the deposit, to ca. 15%.	Orange-yellow weathered, vesicular, crystal poor pumice, sometimes with a mingled appearance. Two lithic types: black, angular, non-vesicular lava-like clast and a black, vesicular scoria.	Pumice fall	K	39°52′S 71°55′W	3	3	75	A	A
MC2		Orange-weathered, fine-lapilli sized pumice deposit	orange-weathered, vesicular, crystal poor pumice	Pumice fall	C	40°00′S 72°0′W	2.6		12		
MC1		Moderately-sorted, slight reverse grading, non-welded, black-red weathered, fine-lapilli to coarse-bombs sized clasts (up to 35 cm) scoria deposit.	Black, dense, vesicular scoria.	Scoria fall from nearby cone	K	39°52′S 71°55′W	35		>200		
MC26		Poorly-moderately-sorted, black, medium-lapilli to bombs sized scoria deposit.	Black, vesicular scoria with abundant xenoliths of a milky-white, medium-grained, crystalline, felsic intrusive rock.	Scoriaceous PDC		39°56′S 72°06′W	>20		>180		
MC27	MC27D	Well-sorted, brown-black weathered scoria deposit	Brown-black, vesicular, microlite rich scoria	Scoria fall. Sub-units may record pulsating activity of the plume	O	39°51′S 72°6′W			33		
	MC27C	Thin, coarse, grey ash with fine laminations. Sharp contact with MF27B and MF27D	Heterogeneous clasts with no modal glass morphology and abundant xenoliths of country rock.						5		
	MC27B	Well-sorted, brown-black weathered, medium-lapilli scoria rich deposit.	Brown-black, slightly vesicular scoria, which is often altered to clay, and xenoliths of country rock.						5		
	MC27A	Thin, fine, grey ash with a sharp contact with MC27B							2		

Units are ordered in stratigraphic order from youngest (MC25; at the top) to oldest (MC1; at the base). MC26 and MC27, described last, have a poor age constraint so are not included within the stratigraphy. Units in Category α, are in bold, those in Category β are unformatted and those pertaining to Category γ are in italics. The letters correspond to the stratigraphic column label in Fig. 2, the associate field photos in Fig. 3 and SEM images in Fig. 4. The maximum pumice (MP), maximum scoria (MS), maximum lithic (ML) and thickness (Th) of the deposit at the type locality are given.

3.2.2. Category β

Deposits assigned to Category β are moderately dispersed and preserved, and typically found at 5–10 localities at distances less than 15 km from the summit. Eight units are assigned to this category: three pumice falls (MC3, MC12 and MC13), four scoria falls (MC8, MC21, MC23 and MC25) and one scoria fall and PDC unit (MC20). A short description of each is given below and in Table 3.

MC3 is a pumice fall deposit found between the villages of Neltume and Puerto Fui. The deposit, dispersed to the north-east, varies in thickness from 75 cm at 12 km ENE of the summit, to 26 cm at 12.5 km north-east of the summit. At some localities it can be identified by the high lithic abundance and/or sharp change in lithic content from ca. 40%, at the base, to ca. 15% above (e.g., Fig. 3A). Locally, MC3 deposits sit conformably on top of a scoria deposit MC1 and below a palaeosol

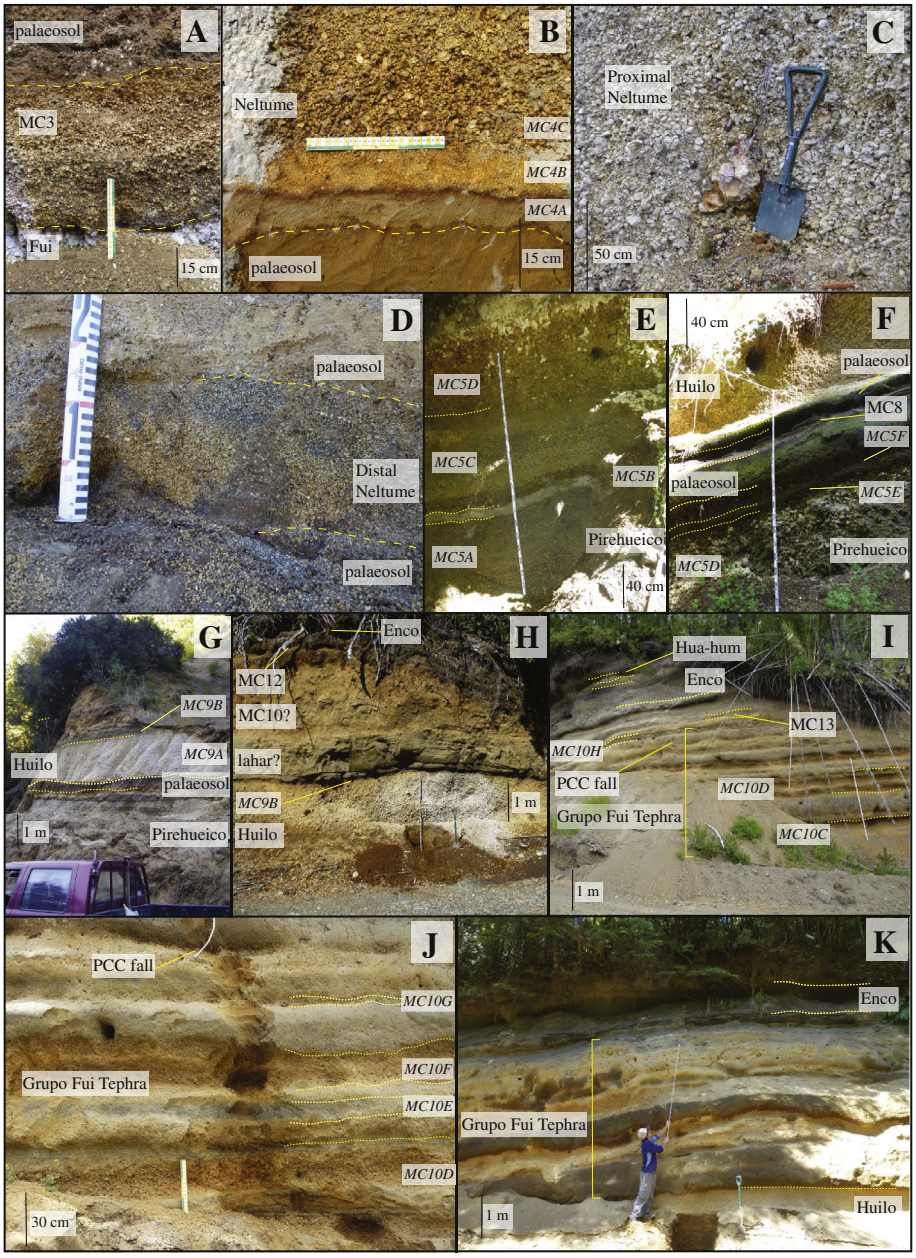

Fig. 3. A. Field photos of deposits around Mocho-Choshuenco. Photos included are just of units comprising Category α and β. GPS coordinates of localities (given by codes in the caption) listed are given in Supplementary material. A: MC3 taken at site 115-01 (column K, Fig. 2); B: the three beds of Neltume (MC4) at 117-01 site (column B, Fig. 2); C: proximal Neltume (MC4) fall deposit, with bombs, at site 302-01; D: distal Neltume (MC4) at site 030114-4 between Quetrupillán and Lanín; E: lower sub-units of Pirehueico (MC5) at site 130114-1 (column E, Fig. 2); F: upper sub-units of Pirehueico (MC5) and lower part of Huilo (MC9) at site 130114-1 (column E, Fig. 2); G: Huilo (MC9) with characteristic scoria band (MC9B) at site 060406-7; H: Huilo with overlying lahar or reworked ash deposit at site 120114-6 (column H, Fig. 2); I: the Grupo Fui Tephra (MC10) with a thin pumice layer from Puyehue-Cordón Caulle (PCC) interbedded within the group at site 115-03 (column J, Fig. 2); J: close-up of the mid-part of MC10 at site 115-03 (column J, Fig. 2); K: Grupo Fui Tephra deposits bounded by Huilo (MC9) and Enco (MC15) deposits at site 130114-1 (column E, Fig. 2). B. Field photos continued. L: Deposits of MC12 and MC13 at site 130108-1 (column G, Fig. 2). Scoria fall is probably from a nearby cone; M: sub-units of Enco (MC15) preserved at site 115-01 (column K, Fig. 2); N: close-up of the packages within MC15D preserved near the Refugio at site 113-01; O: Hua-Hum (MC18) deposits at site 080114-2 (column L, Fig. 2); P: proximal deposits of MC20 at site 080114-6 (column N; Fig. 2); Q: more distal appearance of MC20 and MC18 at site 130129-1; R: Pilmaiquén (MC21) overlying MC20 and within the overlying soil there is scoria from MC25 at site 150114-4; S: Pilmaiquén (MC21) and Riñihue (MC25) at site 130117-1E (column M, Fig. 2); T: Arauco (MC23) and Riñihue (MC25) near the summit at site 070114-8; U: proximal Riñihue (MC25) on the surface of the edifice at site 080114-8 (column P, Fig. 2). The yellow and green ruler is 30 cm long, the tape measure has 10 cm intervals labelled and notches on a 1 cm scale. (For interpretation of the references to colour in this figure legend, the reader is referred to the web version of this article.)

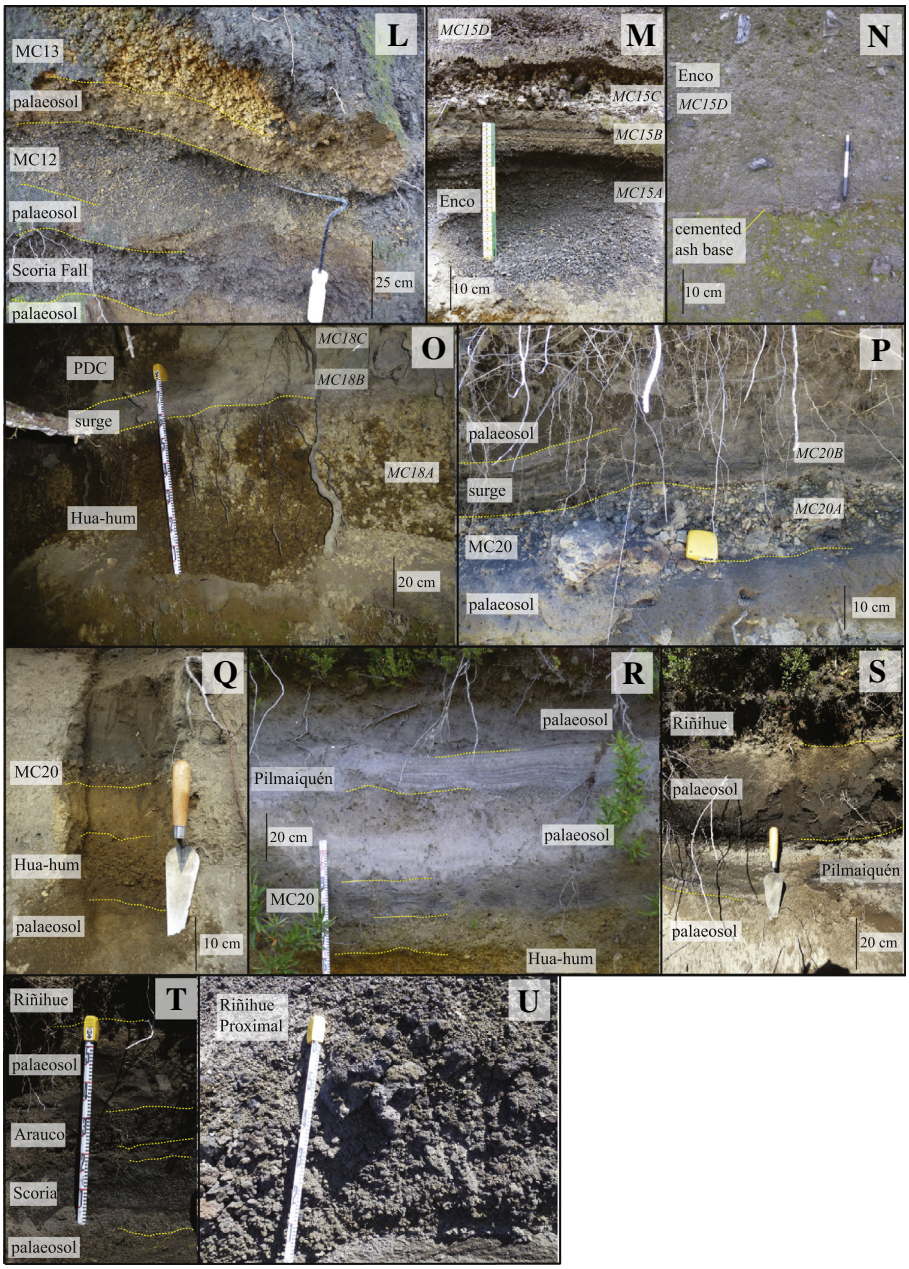

Fig. 3 (*continued*).

(Fig. 3A), which is in turn overlain directly by MC4 (Neltume) deposits. At the type locality (column K, Fig. 2) the overlying palaeosol contains many reworked pumice, scoria and lithic clasts.

MC8 is a red and black scoria deposit found around Pampa-Pilmaiquén. The deposit, probably dispersed to the east, varies in thickness from 15 cm, 10.3 km south-east of the summit, to 90 cm, 11 km north-east. Deposits are intercalated between the pumice deposits of Pirehueico (MC5) and Huilo (MC9; e.g., column E, Fig. 2). The highly oxidised appearance, especially in the lower part of the deposit, may suggest that water was involved in its genesis. The deposits unusually preserve both flow (e.g., cross-bedding) and fall (e.g., rhythmic bedding) features (see Table 3).

MC12 is a pumice fall with deposits dispersed to the north-east where thicknesses of 28 cm, 13.2 km from the summit, and 15 cm, 14.5 km from the summit are preserved., Deposits are always bedded within a palaeosol sequence, and overlying deposits from the Huilo Unit (MC9, e.g., column F, Fig. 2). At a few localities MC12 overlies multiple scoria fall deposits (e.g., column G, Fig. 2) that may comprise part of the Grupo Fui Tephra (MC10) sequence. Typically, MC12 lies beneath deposits from the Enco (MC15) eruption (e.g., column H, Fig. 2). The juvenile clasts in this deposit characteristically have a bimodal appearance; both weather yellow–brown but one is more angular, less vesicular, darker and typically smaller than the second pumice type.

MC13 is an orange-weathered pumice fall deposit, confirmed at four localities, dispersed to the ENE and preserved 11.5 km ENE (64 cm thick) and 11 km ESE (60 cm thick) of the summit. The deposits look very similar to MC9 (Huilo), and are indistinguishable in the field unless the distinctive scoria bed of MC9B is preserved, or the tephra deposit is greater than 1 m thick, in which case it must be part of the MC9 unit; inferred from relative thicknesses preserved at outcrops with both MC9 and MC13 deposits. MC13 deposits lie between deposits from MC10 (The Grupo Fui Tephra) and MC15 (Enco; e.g., column G, J, Fig. 2).

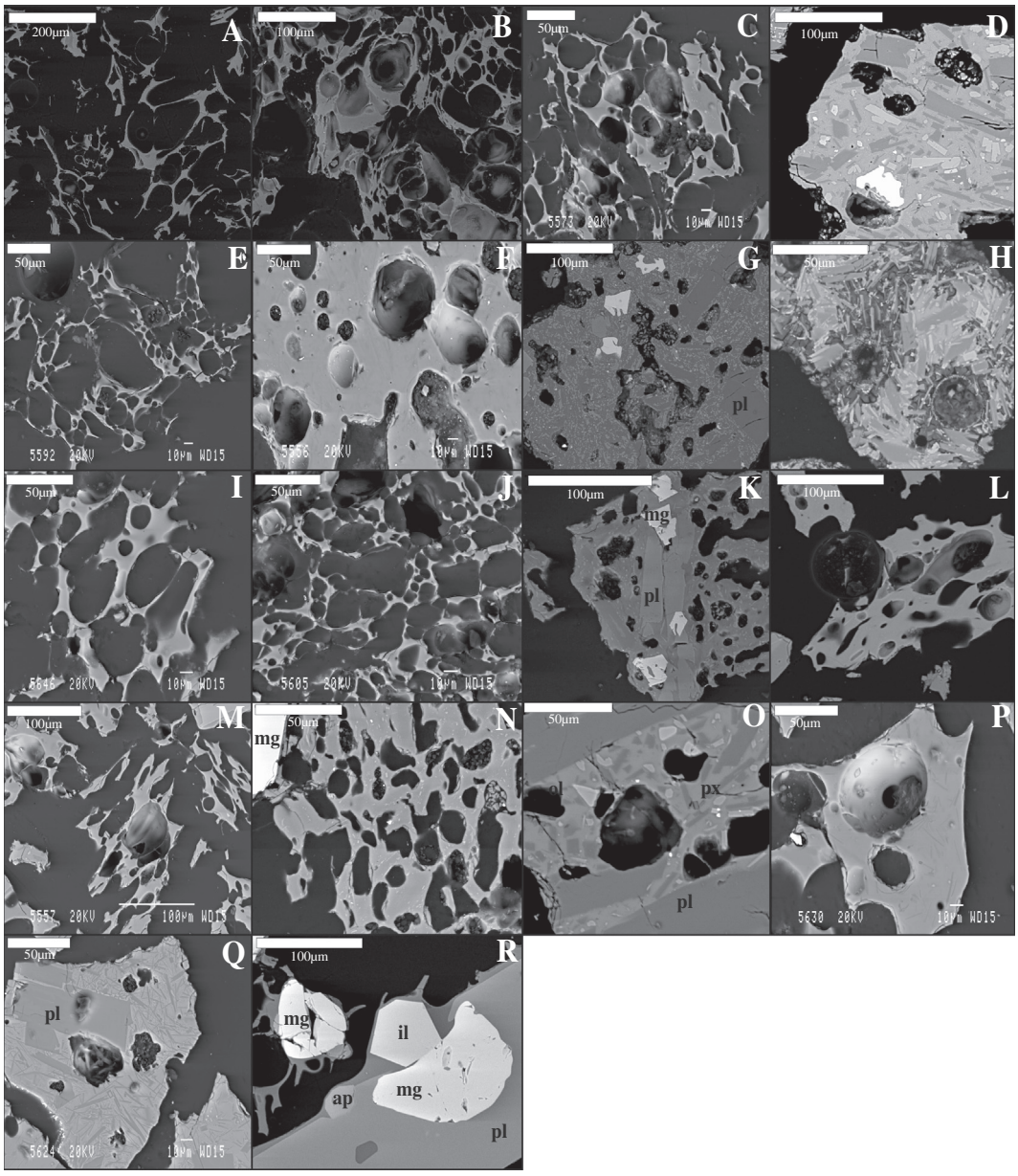

Fig. 4. SEM images of typical glass shards for the tephra units that comprise categories α and β and an example of touching Fe–Ti oxide pairs. A: MC3 pumice; B: MC4B (Neltume) pumice; C: MC5 (Pirehueico) pumice; D: MC8 scoria; E: MC9A (Huilo) pumice; F: MC9B (Huilo) scoria; G: MC10D (Group Fui Tephra) microlite-rich glass; H: MC10C (Grupo Fui Tephra) altered scoria clast; I: MC12 pumice; J: MC13 pumice; K: MC10A (Enco) scoria; L: MC10C (Enco) scoria; M: MC18A (Hua-Hum) pumice; N: MC20A scoria; O: MC21 (Pilmaiquén) scoria; P: MC23 (Arauco) scoria; Q: MC25 (Riñihue) scoria; R: touching Fe–Ti oxide pair in MC4B pumice. Magnetite (mg), ilmenite (il), apatite (ap), plagioclase (pl), pyroxene (px), olivine (ol).

MC20 is a distinctive bi-partite unit comprising two beds, whose appearance differs with proximity to the source (Fig. 3P, Q; described in Table 3). The lower bed, a scoria fall (MC20A), often weathers yellow and is only black in very proximal localities. The upper bed, a PDC (*surge*; MC20B), is typically a grey, medium ash and only preserves characteristic PDC features, such as low-angle cross-bedding, in very proximal sites. Deposits of MC20 are dispersed to the NNE and preserved up to 11 km ESE (10 cm thick) of the summit and 6.2 km ENE (22 cm thick) in Pampa-Pilmaiquén where they overlie the Hua-Hum Unit (MC18), separated by a palaeosol.

MC21 (Pilmaiquén) is a grey, indurated, parallel bedded unit comprising medium ash to fine-lapilli sized clasts (Table 3; columns J and M, Fig. 2; Fig. 3R, S). Beds are continuous, parallel-bedded, well-sorted and often indurated, so we infer that MC21 is the deposit of a wet scoria fall eruption. MC21 deposits commonly overlie MC20, and lie below those from Arauco (MC23) and, more rarely, Riñihue (MC25), all of which are separated by palaeosols. The deposits of MC21 are dispersed to the east and vary in thickness from 18 cm, 11 km ESE of the summit, to 13 cm, 11 km ENE of the summit.

MC23 (Arauco) deposits comprise a well-sorted, massive, scoria deposit (Fig. 3T). At localities on the edifice (e.g., column P, Fig. 2) iridescent scoria bombs (<25 cm) with a black to grey glassy texture are preserved. At the base a thin, grey, coarse lithic-rich ash is sometimes preserved. MC23 deposits typically overlie deposits from Pilmaiquén (MC21) and lie beneath deposits from Riñihue (MC25), all of which are normally separated by palaeosols. The deposits of MC23 are dispersed to the north and vary in thickness from 25 cm, 11.2 km north-east of the summit, to 5 cm, 10.3 km east of the summit.

MC25 (Riñihue) is a scoria fall unit (Fig. 3S–U; Fig. 2, column P) and the youngest deposit found from Mocho-Choshuenco. It lies on the surface of the edifice (thicknesses up to 47 cm are observed) and at rare outcrops to the east (dispersal direction) where it is preserved up to 11 km from the summit (8 cm thick). Deposits are inferred to have formed during the last known eruption from Mocho-Choshuenco in 1864; a thin soil and no other tephra deposits overly these deposits. This fatal eruption reportedly lasted for many days with "*corrientes de fuego*" ("streams of fire") flowing down the valleys mournfully illuminating the elevated waters of Lago Riñihue (Vidal Gormaz, 1869). Local stories describe how the waters of Rio Enco boiled as a result of the eruption, causing the death of a young Mapuche man trying to flee by a canoe (Bernales, 1990). These historic accounts coupled with the preserved deposits comprising well-sorted, vesicular scoria clasts and, on the edifice, bombs (<20 cm diameter) imply that this was probably a Strombolian event.

3.2.3. Category γ

Category γ units are poorly dispersed and preserved. Typically deposits are found at fewer than 5 localities and at distances <15 km from the summit. This group comprises thirteen units, described in Table 3. Primarily units in this group are dark coloured scoria falls (e.g., MC11 and MC22), many of which are likely to originate from one of the many monogenetic cones. However a few units are white–yellow weathered, pumice falls (e.g., MC2 and MC7), which may originate from the main edifice (central vent). Although poorly preserved, MC2 and MC7 may record significant past eruptions as lapilli-size deposits are preserved over 10 km from the Mocho cone. For example, a 12 cm thick, MP of 2.6 cm deposit of MC2 is observed 11 km south-east of the summit (column C, Fig. 2). As these units have limited preservation it is not possible to infer, with any certainty, the dispersal direction or quantify their size.

3.3. Petrography

Most tephra produced at Mocho-Choshuenco is crystal-poor with variable microlite contents and vesicularity. In general the chemically more evolved units (e.g., MC9 (Huilo); ca. 66.7 wt.% SiO_2; Fig. 4E) have a more skeletal morphology with larger (<100 μm) and less spherical vesicles than the more mafic samples. The more mafic samples (e.g., MC25 (Riñihue); ca. 55.5 wt.% SiO_2; Fig. 4Q) tend to have a higher concentration of microlites. The mineralogical assemblage comprises plagioclase, orthopyroxene ± clinopyroxene ± olivine ± magnetite ± ilmenite ± apatite. Rare crystals of chromite and pyrite are also observed.

3.4. Summary of units

We recognise three major pumice fall deposits (MC4 (Neltume), MC5 (Pirehueico) and MC9 (Huilo)) and a large scoria fall and scoriaceous PDC unit (MC15). The MC15 (Enco) unit is very distinctive in the field as it is the only widespread scoria fall deposit from Mocho-Choshuenco, and commonly multiple beds are preserved. The three pumice fall deposits, on the other hand, all have a very similar appearance in the field: orange-weathered, lithic-poor, pumice fall deposits with few other characteristic features. There are few localities where more than one large tephra unit is preserved.

In addition, there are nine further pumice fall deposits (MC1, MC3, MC6, MC7, MC12, MC13, MC18 and MC19), a scoria fall package (MC10), two combined scoria fall and PDC deposits (MC8 and MC20) and a PDC deposit (MC26). The remaining ten units are all scoria fall deposits. The predominance of fall deposits could be due to preservation. Many of the tephra units are overlain by brown–black deposits that include clasts of variable size and composition, which we interpret as palaeosols. High eruptive frequencies, rapid weathering, poor preservation and common reworking mean that it is sometimes difficult to confidently distinguish between palaeosols/weathering horizons, and primary volcanic units, particularly PDCs. Hence it is likely that, despite the high-resolution stratigraphy developed here, we underestimate the scale and frequency of moderate to large eruptions from Mocho-Choshuenco.

The temperate climate and dense vegetation of the region results in exposures often limited to road-cuttings, which makes tracing the deposits from a single event challenging. Measurements of thickness and maximum clast size can help when compared to nearby outcrops where the deposits have been confidently assigned to an event. However, although this approach helps in places (e.g., north of Mocho-Choshuenco and near Coñaripe where only MC4 (Neltume) deposits are preserved), in most areas this is not possible where multiple deposits of a similar appearance are found. This is often the case for MC5 (Pirehueico) and MC9 (Huilo) fall deposits, which are deposits of similar scale that both extend east from the edifice and have similar field parameters in this region. Hence, unless both deposits are preserved in the same locality it is difficult to assign an event to a particular deposit. However, as we show in Section 4, these units are clearly distinguishable chemically.

Pumice samples from the three large eruptions have the same crystal phases: plagioclase, orthopyroxene, clinopyroxene, magnetite, ilmenite and apatite. They are all crystal- and microlite-poor and highly vesicular. Consequently, petrographic observations cannot be used as a diagnostic tool to correlate units. Therefore, to verify stratigraphic correlations, geochemical analyses of glass and Fe–Ti oxides were required.

4. Tephra correlations

4.1. Methods

The deposits were correlated using a combination of field observations (relative stratigraphic position of identified layers, their physical measurements and mapping their geometry) and their composition (glass and mineral chemistry). Outcrops with multiple tephra units preserved (Fig. 2 e.g., columns C, D and F), were chemically analysed first to check whether each unit had a distinct chemical composition, both in terms of glass and Fe–Ti oxides. Outcrops where units had been subsampled were analysed next to check for possible internal chemical variability (Fig. 2 e.g., columns D and H). Once units at these key localities had been well characterised, chemically and physically, and the relative ages determined, the remaining tephra samples were correlated. This was done by using the geochemical characteristics of the units to correlate deposits, which were complemented and verified with field observations (e.g., checking whether the thickness and grain size was consistent with nearby outcrops). At outcrops where samples were not taken, the units were deduced by relative stratigraphic order and physical characteristics (e.g., grain size, thickness and colour).

4.1.1. Chemical analysis

Major element glass compositions of ca. 275 samples were determined with a JEOL JXA-8600 wavelength-dispersive electron microprobe (EMP), equipped with four spectrometers, at the Research Laboratory for Archaeology and the History of Art, University of Oxford. To reduce alkali loss in the glass during analyses, an accelerating voltage of 15 kV, a low beam current (6 nA), and a defocused (10 μm) beam were used. For a few highly vesicular samples a narrower beam (5 μm) was needed and therefore the beam current was reduced (4 nA). Continuity between data from the two beam conditions was checked by analysing a few samples using both setups; no difference was found. Na was analysed first to minimise the effect of possible Na migration. Counts for each element were collected on the peak for 30s (Si, Ca, K, Al, Ti, Fe, Mg), except for Na (10s), P (60s), Mn (40s) and Cl (50s), and background counts were collected for half the time on either side of the peak. The EMP was calibrated using a suite of mineral standards. This calibration was verified using a range of secondary glass standards, which for all runs were

within 2 standard deviations of the preferred values (see Supplementary material; Jochum et al., 2006). Approximately 2150 glass analyses were obtained for which a threshold of 91% was used but totals were mostly >95%. These were normalised to 100% to account for variable secondary hydration (see Supplementary material for raw data and Table 4 for average values). Glass analyses were only possible for ca. 135 samples (i.e., half of those crushed) because of alteration and/or the glass being either too skeletal or microlite-rich.

Magnetite and ilmenite were analysed for ca. 275 samples by EMP with an accelerating voltage of 15 kV, a beam current of 20 nA and a focussed beam. Element counts were collected for 30s (on-peak; Fe, Mg, Al, Si, Ca, Ti) or 40s (Mn). This calibration was verified using a range of secondary mineral standards, which for all runs were within 2 standard deviations of the preferred values (see Supplementary material; Jarosewich et al., 1980). Approximately 2700 analyses were obtained (data presented in Table 5 and Supplementary material) for which totals were typically >94 wt.%, >98.5 wt.% after accounting for the Fe oxidation state so that the stoichiometry is correct (Droop, 1987). All the Fe–Ti oxide pairs presented in this paper (except those noted in 4.2.1.2), are in equilibrium (determined using the method of Bacon and Hirschmann, 1988). Over 600 temperature and oxygen fugacity estimates were calculated using the method of Ghiorso and Evans (2008). As with glass, it was not possible to get Fe–Ti oxide analyses for all samples due to limited abundance and/or size.

4.1.2. Radiocarbon dating

The ages of the explosive eruptions from Mocho-Choshuenco have been constrained through a combination of ^{14}C dating and Bayesian age modelling (e.g., using OxCal; Bronk-Ramsey, 2009a). 48 samples have been ^{14}C-dated, of which 29 were previously published by Lara and Moreno (2007) and 19 new samples were analysed at the NERC Radiocarbon Facility and SUERC AMS laboratory in—East Kilbride using the same methodology outlined in Watt et al., (2011).

Full details of these results including uncalibrated and calibrated ages, can be found in Supplementary material. The ages are calibrated with OxCal 4.2.3 (e.g., Bronk-Ramsey, 2009a) using the Southern Hemisphere ShCal13 curve (Hogg et al., 2013). The dated carbon samples are typically organic-rich palaeosols or small pieces of charcoal within palaeosols bounding the tephra deposits. Most samples are collected below the tephra deposit within the top 5 cm of the palaeosol (Fig. 3; Supplementary material). Only three charcoal samples (within MC15 and MC18; XG-251, 100303-2B and Ch-3; Supplementary material) were recovered from within the deposits themselves. Hence, as most of these samples date the palaeosols that seal, or are sealed by, the eruptive deposits, rather than the eruptions themselves, we create an age model (code included in Supplementary material) to constrain eruption ages. The age model uses a Bayesian statistical approach to combine multiple radiocarbon ages for sequences of events along with constraints provided from field stratigraphy. The approach is outlined by Bronk-Ramsey (2009a, b) and Blockley et al. (2008).

The Bayesian model takes uncalibrated radiocarbon dates as input values. An outlier function was included to identify any radiocarbon analyses that were inconsistent with the age model (e.g., analyses of more modern or reworked older carbon). Three (from 48) radiocarbon dates were found to be outliers, a further three had a <95% probability range and 17 could not be included in the model as they could not be confidently placed within the stratigraphy, and were instead just calibrated. The results from this model are presented in the Supplementary material and Table 6.

4.2. Results

4.2.1. Unit chemistry

Glass and Fe–Ti oxide analyses were attempted for all units (MC1–MC27; Table 3) to aid correlation of the units. The glass geochemistry is plotted in Fig. 5 and summarised in Table 4. The Fe–Ti oxide data and estimated temperature and oxygen fugacity are plotted in Fig. 4 and summarised in Table 5. All raw geochemical data are presented in the Supplementary material.

4.2.1.1. Glass geochemistry. A total of ~2150 glass shards were analysed from 22 tephra units (Fig. 5). Magmas erupted from Mocho-Choshuenco during the last ca. 18 ka are calc-alkaline and range from basaltic andesite to rhyolite in composition. The average major element glass composition is given for each unit in Table 4. The only chemically zoned deposit is MC3, which becomes more evolved up the deposit, from ~60 wt.% SiO_2 at the base to ~70 wt.% SiO_2 towards the top (Fig. 5). The remaining sub-sampled units (MC4, MC5, MC9 and MC18) are relatively compositionally homogeneous and typically span 2 to 3 wt.% SiO_2, which is greater than the calculated error.

Robust chemical correlation ideally requires distinct compositional fields with a narrow distribution from each unit, however this is rarely achieved at volcanoes that are frequently active and experience repeated eruptions across a narrow range of magma compositions (e.g., Smith et al., 2011b). The post-glacial tephra from Mocho-Choshuenco show overlap in glass major element composition between several of the units. Seven units have sufficiently unique major element glass compositions to allow discrimination with just a few glass analyses. Unfortunately, the deposits of the three largest pumice eruptions (MC4, MC5 and MC9) cannot be confidently discriminated using major element glass chemistry alone (Fig. 5).

4.2.1.2. Oxide geochemistry. Analysis of the Fe–Ti oxide compositions of the post-glacial explosive deposits from Mocho-Choshuenco was attempted for all units. A total of ~2700 Fe–Ti oxides were analysed from 19 tephra units (Fig. 6; Table 5). We observe no systematic changes in Fe–Ti oxide chemistry within any eruptive units. Units with a distinct compositional field typically span 2 to 4 wt.% Fe_2O_3 for both the ilmenite and magnetite chemical composition.

Six of the major Mocho-Choshuenco units can be discriminated from each other by Fe–Ti oxide composition alone: MC3, MC4 (Neltume), MC5 (Pirehueico), MC18 (Hua-Hum), MC20 and MC23 (Arauco). Two further units, MC12 and MC9 (Huilo), have compositional fields that overlap with one other unit; MC12 with MC7 and MC9 (Huilo) with MC13. In these cases the stratigraphic position and location relative to the edifice, helps us to distinguish between them: MC12 postdates and MC7 predates both MC9 (Huilo) and MC10 (Grupo Fui Tephra) deposits; MC13 deposits are only found in very proximal localities, compared to MC9 (Huilo) and MC13 glasses are slightly more mafic than those of MC9 (Huilo; Fig. 5). Of the minor events (Category γ), MC2, MC19, MC27 and MC17 all define distinct compositional fields. Fe–Ti oxide data are not sufficient for distinguishing the remaining units, which are typically andesitic, or more mafic in composition. Most major units (categories α and β), with the exception of MC9, MC15, MC21, MC23 and MC25, contain both magnetite and ilmenite. There are a further five minor units (MC17, MC19, MC24, MC26, MC27) that also have no Fe-Ti oxide pairs i.e., the ilmenite phase is not found in samples.

4.2.2. Chronology

In Table 6 we present the first detailed, calibrated chronology for Volcán Mocho-Choshuenco. The earliest post-glacial explosive activity occurred before 14.9–12.2 cal. ka BP (95% confidence level). The four large (volume >1 km^3, see Section 5) explosive eruptions occurred at 12.4–10.4 cal. ka BP (MC4, Neltume), 11.5–8.8 cal. ka BP (MC5, Pirehueico), 8.4–8.0 cal. ka BP (MC9, Huilo) and 1.7–1.5 cal. ka BP (MC15, Enco). These ages supersede previous estimates, which used only uncalibrated ^{14}C dates to constrain eruption ages (e.g., Moreno and Lara, 2007). Our new age model, coupled with the high-resolution stratigraphy, gives further constraints on the tempo of volcanism from Mocho-Choshuenco. The geological record preserves, on average, one explosive event every ~440 years (34 events including the 8 eruptions

Table 4
Major element composition (average and *standard deviation*) of the matrix glass (anhydrous) from the Mocho-Choshuenco tephra deposits.

Eruption	MC25 (Riñihue)		MC24		MC23 (Arauco)		MC22		MC20		MC19		MC18B (Hua-Hum)		MC15C (Enco)		MC14		MC13		MC12		MC11	
SiO_2	55.55	*0.78*	60.19	*0.49*	59.27	*0.47*	59.78	*0.24*	65.02	*0.38*	65.31	*1.35*	63.43	*0.96*	60.94	*0.68*	60.28	*1.14*	65.46	*1.40*	64.34	*2.17*	60.11	*0.42*
TiO_2	1.40	*0.18*	1.38	*0.06*	1.44	*0.08*	1.90	*0.05*	1.09	*0.06*	1.04	*0.10*	1.13	*0.09*	1.29	*0.08*	1.37	*0.14*	0.90	*0.14*	0.98	*0.19*	1.81	*0.13*
Al_2O_3	16.13	*0.73*	15.67	*0.31*	15.60	*0.27*	13.56	*0.28*	15.56	*0.30*	15.44	*0.44*	16.15	*0.47*	16.11	*0.49*	16.35	*0.85*	16.09	*0.29*	15.97	*0.57*	14.22	*0.87*
FeO*	9.19	*0.54*	7.84	*0.35*	8.51	*0.41*	10.03	*0.30*	5.17	*0.27*	5.09	*0.68*	5.59	*0.47*	7.06	*0.49*	7.45	*0.57*	4.53	*0.74*	5.67	*1.04*	9.15	*0.78*
MnO	0.18	*0.04*	0.17	*0.04*	0.19	*0.04*	0.20	*0.06*	0.17	*0.03*	0.14	*0.05*	0.16	*0.05*	0.18	*0.05*	0.18	*0.04*	0.15	*0.05*	0.17	*0.06*	0.19	*0.06*
MgO	4.55	*0.46*	2.69	*0.16*	2.79	*0.11*	2.46	*0.14*	1.49	*0.15*	1.45	*0.23*	1.73	*0.24*	2.30	*0.33*	2.15	*0.42*	1.46	*0.41*	1.36	*0.62*	2.42	*0.43*
CaO	7.86	*0.50*	5.42	*0.26*	5.78	*0.18*	5.74	*0.21*	3.86	*0.11*	4.00	*0.62*	4.30	*0.40*	5.24	*0.30*	5.43	*0.63*	3.77	*0.59*	3.74	*0.99*	5.39	*0.41*
Na_2O	3.83	*0.26*	4.59	*0.26*	4.75	*0.20*	4.23	*0.27*	5.40	*0.17*	5.41	*0.19*	5.34	*0.25*	5.00	*0.30*	4.97	*0.27*	5.59	*0.47*	5.46	*0.45*	4.40	*0.30*
K_2O	1.00	*0.17*	1.62	*0.11*	1.27	*0.06*	1.59	*0.08*	1.77	*0.08*	1.70	*0.15*	1.65	*0.17*	1.40	*0.16*	1.38	*0.17*	1.66	*0.17*	1.90	*0.25*	1.73	*0.13*
P_2O_5	0.26	*0.06*	0.33	*0.03*	0.34	*0.03*	0.41	*0.03*	0.34	*0.02*	0.30	*0.04*	0.39	*0.06*	0.37	*0.05*	0.35	*0.05*	0.25	*0.06*	0.37	*0.08*	0.45	*0.06*
Cl	0.06	*0.02*	0.09	*0.02*	0.06	*0.05*	0.11	*0.02*	0.13	*0.02*	0.12	*0.02*	0.14	*0.03*	0.10	*0.03*	0.10	*0.03*	0.15	*0.03*	0.14	*0.04*	0.12	*0.02*
H_2O**	0.20	*0.93*	−0.02	*0.48*	0.84	*0.90*	0.53	*0.28*	2.43	*1.13*	2.38	*0.90*	0.06	*1.65*	0.82	*1.36*	1.15	*0.59*	0.31	*1.74*	−0.10	*1.39*	−0.04	*0.65*
N	124		29		140		9		13		19		156		340		26		31		183		21	

Average and standard deviations (italics) for tephra deposits. Compositions in weight percent (wt.%) were determined using a wavelength-dispersive EMP (see Section 4.1). N = number of analyses, **H_2O by difference. See Supplementary material for the ca. 2150 raw analyses. Glass analysis was not possible for all samples. For the more evolved samples (i.e., the dacites and rhyolites) this was as a result of extensive weathering (e.g., the deposits in Argentina) or the material being too highly vesicular, which is often the case with MC9 (Huilo) pumice (vesicle walls commonly thinner than 1 μm). For the more mafic samples (i.e., basaltic andesites and basalts; particularly the scoria from the cones) the microlite density was often too high (e.g., Fig. 4G) for glass analysis to be possible. Therefore the melt chemistry is likely to be biased towards the more silicic compositions.

Table 4 (*continued*)

Eruption	MC10 (Grupo Fui Tephra)		MC9B (Huilo)		MC9A (Huilo)		MC8		MC7		MC6		MC5 (Pirehueico)		MC4C (Neltume)		MC3		MC2		MC1	
SiO_2	55.80	*0.74*	60.93	*0.29*	66.69	*0.96*	58.70	*0.91*	64.84	*0.71*	68.01	*0.55*	69.13	*1.06*	70.12	*0.69*	64.78	*3.31*	71.46	*0.69*	53.69	*0.40*
TiO_2	1.51	*0.13*	1.20	*0.05*	0.78	*0.09*	1.45	*0.19*	1.01	*0.09*	0.72	*0.06*	0.63	*0.08*	0.51	*0.08*	0.81	*0.18*	0.42	*0.07*	1.88	*0.13*
Al_2O_3	15.55	*0.63*	16.47	*0.15*	16.04	*0.30*	16.35	*0.87*	15.42	*0.47*	15.97	*0.30*	15.55	*0.45*	15.29	*0.31*	15.92	*0.79*	14.85	*0.37*	15.02	*0.58*
FeO*	9.78	*0.61*	6.51	*0.25*	3.88	*0.47*	8.04	*0.69*	5.77	*0.35*	3.36	*0.28*	3.03	*0.40*	2.89	*0.35*	5.33	*1.47*	2.65	*0.24*	10.16	*0.64*
MnO	0.19	*0.04*	0.18	*0.03*	0.15	*0.05*	0.17	*0.05*	0.18	*0.05*	0.14	*0.04*	0.12	*0.05*	0.12	*0.04*	0.14	*0.05*	0.09	*0.05*	0.18	*0.04*
MgO	4.14	*0.42*	2.40	*0.07*	1.09	*0.19*	2.28	*0.82*	1.23	*0.16*	0.84	*0.11*	0.71	*0.19*	0.56	*0.09*	1.56	*0.65*	0.40	*0.08*	4.33	*0.28*
CaO	7.79	*0.47*	5.15	*0.15*	3.12	*0.39*	6.39	*0.56*	3.67	*0.30*	2.57	*0.20*	2.26	*0.41*	2.01	*0.22*	4.22	*1.33*	1.71	*0.18*	8.36	*0.40*
Na_2O	3.81	*0.26*	5.24	*0.22*	6.07	*0.30*	4.94	*0.34*	5.46	*0.17*	6.06	*0.19*	5.97	*0.27*	5.84	*0.25*	5.10	*0.40*	5.60	*0.18*	3.89	*0.37*
K_2O	1.10	*0.12*	1.37	*0.07*	1.81	*0.12*	1.13	*0.18*	1.93	*0.15*	1.99	*0.12*	2.26	*0.16*	2.37	*0.10*	1.86	*0.39*	2.54	*0.12*	1.80	*0.26*
P_2O_5	0.28	*0.03*	0.43	*0.03*	0.20	*0.05*	0.48	*0.07*	0.34	*0.04*	0.16	*0.03*	0.15	*0.04*	0.10	*0.04*	0.14	*0.04*	0.07	*0.03*	0.60	*0.06*
Cl	0.06	*0.01*	0.11	*0.02*	0.18	*0.03*	0.08	*0.02*	0.15	*0.03*	0.18	*0.03*	0.20	*0.03*	0.19	*0.03*	0.13	*0.04*	0.20	*0.02*	0.09	*0.02*
H_2O**	1.76	*0.73*	0.19	*0.66*	0.31	*1.79*	0.80	*0.83*	−0.13	*0.54*	−0.16	*0.64*	0.84	*1.73*	1.12	*2.06*	1.14	*1.43*	0.19	*0.69*	0.36	*0.56*
N	64		26		179		19		34		21		262		282		110		28		13	

Table 5
Major element compositions (average and *standard deviation*) of the Fe–Ti oxides from the Mocho-Choshuenco tephra deposits.

Eruption		MC27		MC26		MC24		MC23 (Arauco)		MC21 (Pilmaiquén)		MC20		MC19		MC18B (Hua-Hum)		MC17		MC16		MC15C (Enco)	
Magnetite	SiO_2	0.08	*0.02*	0.06	*0.05*	0.06	*0.02*	0.07	*0.02*	0.11	*0.13*	0.05	*0.02*	0.06	*0.06*	0.05	*0.02*	0.05	*0.02*	0.14	*0.14*	0.07	*0.05*
	TiO_2	12.59	*0.35*	11.97	*2.92*	13.01	*1.10*	11.52	*0.19*	12.05	*2.82*	13.12	*0.33*	14.54	*0.28*	13.54	*0.79*	15.71	*0.34*	12.79	*1.76*	13.57	*4.90*
	Al_2O_3	3.54	*0.13*	3.17	*0.87*	3.12	*0.38*	3.81	*0.09*	3.48	*0.83*	2.91	*0.11*	2.77	*0.08*	3.15	*0.23*	2.87	*0.16*	3.69	*0.55*	3.39	*0.63*
	FeO*	73.81	*0.85*	75.83	*3.57*	74.31	*0.45*	74.62	*0.49*	74.47	*3.57*	74.72	*0.92*	73.76	*0.37*	74.17	*1.16*	72.39	*0.63*	73.06	*1.58*	73.68	*4.07*
	MnO	0.44	*0.04*	0.54	*0.20*	0.46	*0.07*	0.40	*0.03*	0.38	*0.05*	0.65	*0.04*	0.57	*0.03*	0.56	*0.05*	0.59	*0.03*	0.42	*0.05*	0.48	*0.06*
	MgO	3.41	*0.34*	2.96	*0.92*	3.30	*0.28*	3.60	*0.08*	3.12	*0.66*	2.85	*0.18*	3.15	*0.19*	3.29	*0.24*	2.80	*0.20*	3.29	*0.26*	3.48	*0.40*
	CaO	0.08	*0.03*	0.04	*0.04*	0.02	*0.02*	0.02	*0.01*	0.12	*0.06*	0.03	*0.02*	0.03	*0.03*	0.03	*0.04*	0.02	*0.01*	0.11	*0.06*	0.05	*0.05*
	Total	93.95	*0.75*	94.56	*1.74*	94.28	*0.63*	94.03	*0.55*	93.72	*1.34*	94.32	*1.12*	94.89	*0.48*	94.78	*0.88*	94.44	*0.82*	93.50	*0.67*	94.71	*1.31*
	FeO	37.08	*0.71*	37.30	*2.35*	37.68	*1.41*	36.02	*0.31*	37.02	*2.11*	38.23	*0.68*	39.27	*0.63*	38.20	*0.73*	40.65	*0.53*	37.38	*1.65*	37.50	*1.75*
	Fe_2O_3	40.82	*0.94*	42.81	*5.63*	40.70	*1.59*	42.89	*0.43*	41.61	*5.74*	40.55	*0.64*	38.33	*0.48*	39.97	*1.60*	35.28	*0.67*	39.65	*3.46*	40.21	*4.72*
	Total	97.96	*0.82*	98.81	*1.57*	98.30	*0.54*	98.26	*0.58*	97.78	*1.21*	98.34	*1.16*	98.67	*0.48*	98.74	*0.91*	97.97	*0.85*	97.33	*0.99*	98.68	*1.11*
	N	18		50		18		39		26		53		18		402		17		13		182	
Ilmenite	SiO_2			0.00	*0.01*							0.00	*0.01*			0.00	*0.01*	0.00	*0.00*				
	TiO_2			45.02	*1.40*							44.77	*0.39*			45.42	*0.69*	47.02	*0.27*				
	Al_2O_3			0.24	*0.11*							0.35	*0.03*			0.34	*0.03*	0.36	*0.03*				
	FeO*			47.31	*1.20*							48.31	*0.46*			46.96	*0.80*	45.35	*0.04*				
	MnO			1.47	*1.07*							0.68	*0.05*			0.63	*0.05*	0.58	*0.06*				
	MgO			2.87	*0.99*							3.78	*0.30*			4.16	*0.34*	4.40	*0.42*				
	CaO			0.06	*0.02*							0.05	*0.04*			0.07	*0.11*	0.10	*0.09*				
	Total			96.96	*1.53*							97.96	*0.68*			97.57	*0.73*	97.81	*0.01*				
	FeO			33.83	*1.50*							32.78	*0.67*			32.74	*0.76*	33.73	*0.82*				
	Fe_2O_3			14.98	*2.15*							17.26	*0.65*			15.80	*1.05*	12.91	*0.86*				
	Total			98.46	*1.44*							99.68	*0.70*			99.15	*0.73*	99.10	*0.07*				
	N			8								28				27		2					
Temperature (°C)												963	*9*			955	*12*	954	*11*				
$\log_{10}(fO_2)$												0.55	*0.04*			0.38	*0.08*	0.03	*0.13*				

Average and standard deviations (*italics*) for tephra deposits. Compositions in weight percent (wt%) were determined using a wavelength-dispersive EMP (see Section 4.1). N = number of analyses. FeO and Fe_2O_3 calculated as in Droop (1987). Temperature (T) and oxygen fugacity (fO_2) calculated as in Ghiorso and Evans (2008). See Supplementary material for the ca. 2700 raw analyses.

Table 5 (*continued*)

Eruption		MC13		MC12		MC9B (Huilo)		MC9A (Huilo)		MC7		MC6		MC5 (Pirehueico)		MC4 (Neltume)		MC3		MC2	
Magnetite	SiO_2	0.04	*0.02*	0.05	*0.02*	0.04	*0.02*	0.04	*0.03*	0.05	*0.02*	0.04	*0.01*	0.05	*0.08*	0.05	*0.09*	0.04	*0.02*	0.03	*0.01*
	TiO_2	12.20	*0.21*	17.24	*0.32*	13.40	*6.67*	12.31	*0.20*	17.14	*0.29*	12.56	*0.12*	11.44	*0.38*	13.21	*1.53*	14.17	*3.46*	14.15	*0.28*
	Al_2O_3	2.64	*0.09*	2.67	*0.07*	2.90	*0.88*	2.65	*0.10*	2.67	*0.04*	2.49	*0.07*	2.40	*0.10*	2.07	*0.21*	2.11	*0.21*	1.98	*0.16*
	FeO*	75.98	*0.47*	72.06	*0.54*	74.13	*5.80*	75.98	*0.77*	72.57	*0.34*	75.79	*0.52*	76.91	*1.13*	76.57	*1.68*	76.03	*3.14*	76.52	*0.37*
	MnO	0.79	*0.04*	0.65	*0.03*	0.71	*0.15*	0.78	*0.04*	0.66	*0.03*	0.77	*0.03*	0.83	*0.04*	0.85	*0.08*	0.79	*0.05*	0.83	*0.05*
	MgO	2.74	*0.10*	2.61	*0.09*	3.07	*0.52*	2.74	*0.11*	2.64	*0.06*	2.56	*0.07*	2.35	*0.10*	1.84	*0.24*	2.06	*0.17*	1.60	*0.20*
	CaO	0.03	*0.05*	0.05	*0.10*	0.05	*0.12*	0.03	*0.05*	0.04	*0.06*	0.02	*0.02*	0.03	*0.04*	0.02	*0.03*	0.02	*0.03*	0.03	*0.04*
	Total	94.43	*0.58*	95.33	*0.65*	94.29	*0.79*	94.54	*0.83*	95.76	*0.42*	94.25	*0.52*	94.01	*1.31*	94.61	*0.85*	95.22	*1.02*	95.15	*0.34*
	FeO	37.45	*0.40*	42.45	*0.50*	36.65	*1.81*	37.59	*0.41*	42.48	*0.40*	37.98	*0.28*	37.18	*0.67*	39.63	*1.15*	40.02	*0.86*	41.41	*1.56*
	Fe_2O_3	42.82	*0.34*	32.90	*0.58*	41.65	*5.11*	42.67	*0.55*	33.44	*0.49*	42.01	*0.42*	44.15	*0.85*	41.05	*2.93*	40.02	*2.82*	39.02	*1.74*
	Total	98.70	*0.59*	98.58	*0.66*	98.42	*0.48*	98.78	*0.87*	99.06	*0.43*	98.41	*0.55*	98.39	*1.37*	98.68	*0.82*	99.19	*0.98*	99.02	*0.41*
	N	81		122		23		274		17		11		250		446		88		13	
Ilmenite	SiO_2	0.01	*0.03*	0.00	*0.01*	0.00	*0.00*	0.01	*0.02*	0.00	*0.00*	0.00	*0.00*	0.00	*0.01*	0.00	*0.02*	0.00	*0.00*	0.00	*0.00*
	TiO_2	44.67	*0.42*	48.38	*0.35*	44.76	*0.36*	44.80	*0.40*	48.40	*0.26*	45.31	*0.41*	44.90	*0.39*	47.07	*0.46*	47.17	*1.05*	47.64	*0.30*
	Al_2O_3	0.30	*0.02*	0.26	*0.01*	0.30	*0.01*	0.30	*0.03*	0.25	*0.02*	0.27	*0.02*	0.25	*0.02*	0.18	*0.02*	0.20	*0.01*	0.15	*0.02*
	FeO*	47.67	*0.38*	45.40	*0.33*	47.51	*0.26*	47.71	*0.43*	45.46	*0.17*	47.24	*0.31*	47.64	*0.51*	46.77	*0.46*	46.72	*0.59*	46.82	*0.39*
	MnO	0.87	*0.05*	0.72	*0.04*	0.81	*0.06*	0.85	*0.06*	0.73	*0.03*	0.90	*0.04*	0.98	*0.06*	1.09	*0.07*	0.93	*0.06*	1.11	*0.11*
	MgO	4.02	*0.09*	3.73	*0.12*	4.05	*0.05*	3.98	*0.17*	3.68	*0.09*	3.81	*0.18*	3.59	*0.18*	3.06	*0.17*	3.49	*0.35*	2.64	*0.26*
	CaO	0.04	*0.04*	0.04	*0.04*	0.05	*0.05*	0.05	*0.07*	0.04	*0.01*	0.04	*0.03*	0.05	*0.07*	0.03	*0.03*	0.03	*0.02*	0.04	*0.03*
	Total	97.58	*0.62*	98.54	*0.56*	97.47	*0.49*	97.70	*0.63*	98.57	*0.34*	97.57	*0.37*	97.39	*0.54*	98.21	*0.67*	98.54	*1.32*	98.39	*0.30*
	FeO	32.09	*0.45*	36.10	*0.39*	32.17	*0.26*	32.29	*0.51*	36.20	*0.35*	33.01	*0.64*	32.95	*0.46*	35.75	*0.59*	35.24	*0.80*	36.98	*0.57*
	Fe_2O_3	17.31	*0.52*	10.34	*0.54*	17.04	*0.43*	17.14	*0.65*	10.30	*0.22*	15.82	*0.76*	16.32	*0.70*	12.24	*0.80*	12.75	*0.79*	10.94	*1.04*
	Total	99.32	*0.62*	99.57	*0.57*	99.17	*0.49*	99.41	*0.65*	99.60	*0.32*	99.15	*0.35*	99.02	*0.56*	99.43	*0.70*	99.82	*1.27*	99.49	*0.39*
	N	28		40		8		141		3		8		141		128		28		7	
Temperature (°C)		933	*6*	932	*6*	930	*9*	934	*8*	924	*1*	924	*11*	903	*11*	888	*12*	905	*9*	876	*16*
$\log_{10}(fO_2)$		0.54	*0.03*	−0.36	*0.10*	0.51	*0.03*	0.53	*0.05*	−0.37	*0.06*	0.41	*0.06*	0.48	*0.08*	−0.04	*0.11*	0.06	*0.06*	−0.26	*0.19*

Table 6
Summary of the stratigraphic relationship and characteristics of the explosive units.

Eruption		Unit type	Chemical analyses	Dispersal	Volume (km^3)	Mass (kg)	Magnitude	Column Height (km)	Wind Speed (ms^{-1})	Modelled age cal. yrs BP
MC25 (Riñihue)		Basaltic–andesite fall	**Glass**	E			~3			**278–48**
MC24		Andesitic fall	**Glass** & oxides	E?			~<3			**374–96**
MC23 (Arauco)		Andesitic fall	**Glass** & oxides	N			~3			**460–215**
MC22		Andesitic fall	**Glass**	E?			~<3			**495–325**
MC21 (Pimaiquén)		Wet scoria fall	**Oxides**	E			~4			**543–365**
MC20		Dacitic fall and overlying PDC	Glass & **oxides**	NNE			~4			**1228–842**
MC19		Andesite–dacitic fall	Glass & **oxides**	NE?			~<3			**1328–1061**
MC18 (Hua–hum)		Andesite–dacitic fall	Glass & **oxides**	NE & SE	0.4	4.0E+11	4.6	~30	~30	**1375–1155**
MC17		Scoria fall	**Oxides**	NE?			~<3			**1490–1303**
MC16		Scoria fall	**Oxides**	NE?			~<3			**1624–1340**
MC15 (Enco)	MC15D	Andesitic PDC	**Glass** & oxides	Radial	1	1.5E+12	5.0			**1695–1465**
	MC15C	Andesitic fall	**Glass** & oxides	SE	0.7	1.1E+12		~30	~30	
MC14		Andesitic cone eruption	**Glass**	E?			~3			**2083–1594**
MC13		Dacitic fall	Glass & **oxides**	ENE			~4			**2324–1806**
MC12		Andesite–dacitic fall	Glass & **oxides**	NE			~4			**2832–2158**
MC11		Andesitic fall	**Glass**	E?			~3			**3494–2302**
MC10 (Grupo Fui Tephra)	MC10H	Scoria fall package	**Glass**	NE, E, SE			~3			**3692–2755**
	MC10G						~3			**5415–3580**
	MC10F						~3			**6053–3770**
	MC10E						~3			**6613–4105**
	MC10D						~3			**7065–4555**
	MC10C						~3			**7413–5101**
	MC10B						~3			**7628–5685**
	MC10A						~3			**8001–6577**
MC9 (Huilo)		Dacitic fall	Glass & **oxides**	E	2.2	2.2E+12	5.3	~30	~30	**8422–7982**
MC8		Andesitic cone eruption	**Glass**	E?			~3			**8896–8321**
MC7		Andesite–dacitic fall	Glass & **oxides**	E?			~3			**9166–8396**
MC6		Dacitic fall?	Glass & **oxides**	E?			~3			**9381–8561**
MC5 (Pirehueico)		Rhyolite–dacitic fall	Glass & **oxides**	E	2.0	2.0E+12	5.3	~30–35	~40	**11549–8828**
MC4 (Neltume)		Rhyolitic fall	Glass & **oxides**	NNE	5.3	5.3E+12	5.7	~30–35	~35	**12393–10389**
MC3		Zoned fall	**Glass** & oxides	NE			~4			**13208–11999**
MC2		Rhyolitic fall	Glass & **oxides**	SE?			~3			**14145–12073**
MC1		Basaltic–andesite cone eruption	**Glass**	NE?			~3			**14918–12183**
Relative stratigraphy not well constrained										
MC26		Tumba Buey Cone scoria fall and flow	**Oxides**	W						**Post–dating MC15**
MC27		Scoria fall	**Oxides**	NW?						**Between MC4 and MC23**

Chemical analyses highlights the geochemical analyses that were possible on the deposits with the better phase for correlation in bold. Eruption sizes are estimated using AshCalc (Daggit et al., 2014) and the exponential thickness decay mode (e.g., Pyle, 1989; Fierstein and Nathenson, 1992) and magnitude equation of Pyle (2000). For evolved deposits, with a density of ~1000 kg/m^3, the VEI and magnitude estimates are identical. For more mafic, dense deposits (e.g., density of ~1500 kg/m^3) the magnitude estimates are higher; a VEI 3–4 eruption would have a magnitude of 3.2–4.2. For units with limited exposure magnitudes are estimated by general thickness and grain size and compared to similar units in the literature. Question marks and tildes (~) are used where there is uncertainty due to limited preservation.

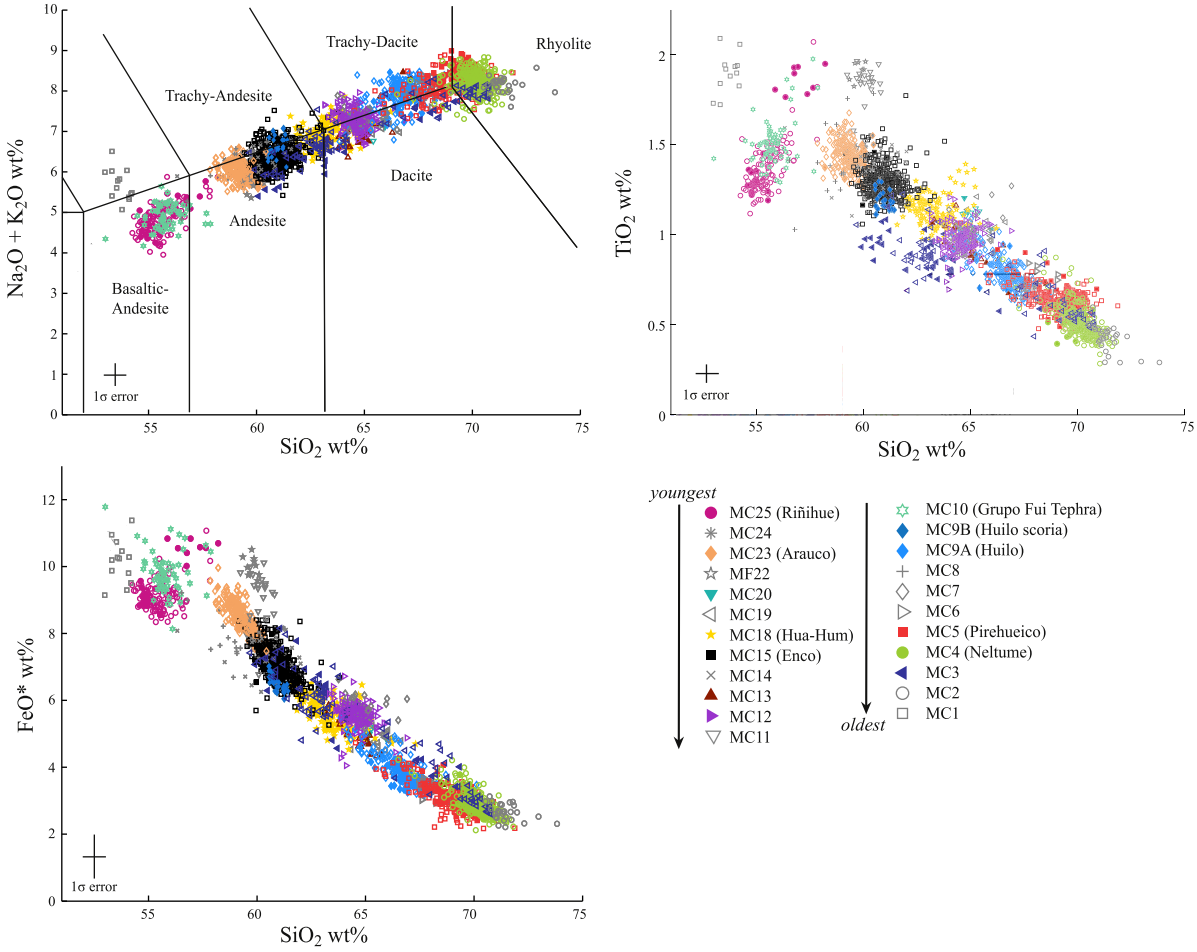

Fig. 5. Major element composition for the matrix glass (anhydrous) for the different tephra units from Mocho-Choshuenco. The different colours and/or symbols represent the data from different units, as labelled in the legend. The filled symbols represent data from the type localities for category α and β units, as defined in Table 3. All the units that form part of categories α and β are given coloured symbols whereas units in Category γ are grey. The error bars are calculated from the relative percentage errors on the compositionally similar secondary standards. (For interpretation of the references to colour in this figure legend, the reader is referred to the web version of this article.)

within Grupo Fui Tephra). However, when taking all the monogenetic cone deposits (ca. 40 eruptions) into account the complex is more active with one explosive event preserved every ~220 years.

4.3. Discussion

By combining field stratigraphy, glass and Fe–Ti oxide compositional data, we are able to identify and chemically fingerprint 27 explosive units (34 eruptions) from Mocho-Choshuenco from post-glacial times, and confirm the existence of three, rather than two (Moreno and Lara, 2007), major dacitic pumice fall deposits. In turn, these data provide a more complete picture of the style, frequency, distribution and size of past explosive eruptions. This is invaluable not just for evaluating potential future volcanic hazards, but also for understanding how the system has changed over time and may have been affected by changes in the regional climatic and/or tectonic regimes.

5. Eruption sizes

Having established tools to discriminate between the deposits of different eruptions, we now explore constraints on eruption size and frequency from the dispersal and grain size characteristics of the deposits. Measurements of unit thickness, maximum pumice, scoria and lithic sizes enable eruption parameters, such as eruption volume, column height, dispersal and magnitude to be estimated (Carey and Sparks, 1986; Pyle, 1989, 1995, 2000). The eruptive parameters were determined for the five most widely dispersed and well preserved fall units: MC4 (Neltume), MC5 (Pirehueico), MC9 (Huilo), MC15 (Enco) and MC18 (Hua-Hum).

Fall deposit volumes were estimated by constructing isopach maps (Fig. 7) and plotting the ln (thickness) against the square root of the isopach area. Deposit volumes were determined with the *AshCalc* tool (Daggitt et al., 2014), using the exponential thickness decay model of Pyle (1989, 1995), with one (MC9A, MC15C, MC18A) or two (MC4C, MC5) segments (Fierstein and Nathenson, 1992). The absence of distal material and post-depositional compaction means that the volume estimates represent minimal values. Total (preserved) deposit mass was determined using an assumed (medial) deposit density of 1000 kg/m^3 for Neltume (MC4), Pirehueico (MC5), Huilo (MC9) and Hua-Hum (MC18), and 1500 kg/m^3 for Enco (MC15) as denser scoria and more abundant lithics are present in the deposit. These assumed density values have been estimated for similar tephra deposits by Scasso et al. (1994) and Cobeñas et al. (2012). The estimates were then used to calculate the approximate magnitude of these eruptions, using the relationship magnitude = $\log_{10}$[erupted mass, kg] − 7 (Pyle, 2000). Eruption column heights were estimated using the Carey and Sparks (1986) model, based on the maximum pumice isopleths (MP and ML measurements included in Supplementary material). As a result of pumice clasts breaking upon impact and unconstrained pumice density the eruption column heights are considered indicative rather than

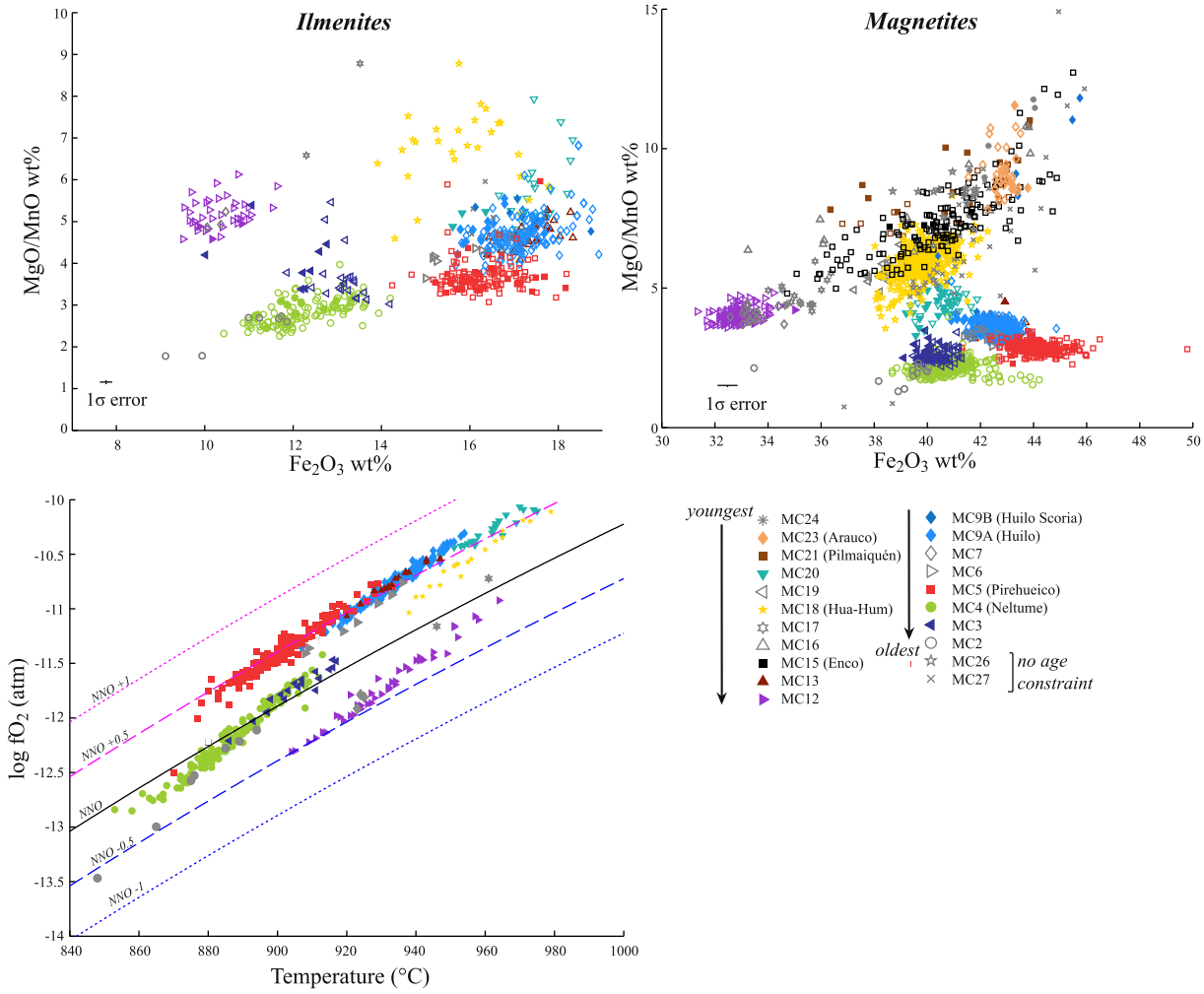

Fig. 6. Fe–Ti oxide (magnetite and ilmenite) composition of the different Mocho-Choshuenco tephra units. The notation is the same as in Fig. 5 with the filled symbols representing data from the type localities for category α and β units, as defined in Table 3. The error bars are calculated from the relative percentage errors on the secondary standards. The bottom left graph is the temperature and log (fO_2) estimates, determined using Ghiorso and Evans (2008) Fe–Ti oxide geothermometer plotted with respect to the Ni–Ni–O (NNO) buffer. All units have filled symbols for temperature and oxygen fugacity estimates.

absolute. Maximum lithic measurements, although taken, unfortunately were too sparse and variable to construct isopleths. Estimates of eruption volume, mass, magnitude and column height are presented in Table 6 along with the dispersal direction and modelled ages for the 27 units identified.

Four deposits exceed magnitude 5: MC4 (Neltume), MC5 (Pirehueico), MC9 (Huilo) and MC15 (Enco). The Neltume unit (MC4) is the largest and oldest of these four events (magnitude ~5.7). Its deposits are abundant and narrowly dispersed to the NNE (Fig. 7A). Enco (MC15), the second largest and youngest of the large units, comprises a sub-Plinian fall and PDC deposit, with a combined magnitude of ~5.4. The PDC deposit volume was estimated from field thickness measurements and measuring the area of valleys, on Google Earth, where deposits were found. Deposits (PDC and fall) from this event are widespread radially around the volcano (Fig. 7D). The Huilo unit (MC9) is the third largest unit preserved (magnitude ~5.3). Deposits are relatively abundant and quite broadly dispersed to the east (Fig. 7C). Pirehueico (MC5) is the smallest of the four large units (magnitude ~5.3) with deposits dispersed to the east (Fig. 7B).

As well as four units having a magnitude >5, six units are estimated to have a magnitude ~4, 19 units (including the 8 within Grupo Fui Tephra) have a magnitude ~3 and five units have a magnitude ~<3 (Table 6). For units with magnitude <5 these estimates are indicative as they are not based on isopach measurements, due to absence of data, instead they are approximated from comparing their thickness, with distance from the edifice, to well constrained events. The 27 units (34 eruptions) have a combined estimated volume of ~16 km^3 of pyroclastic material. Using the monogenetic cone dimensions given in Moreno and Lara (2007), i.e., base diameter 1250 m, height 150–250 m and crater diameter of 200–750 m, the cones are estimated to contribute a further ~4 km^3 of pyroclastic material. Therefore it is estimated that ≥20 km^3 of pyroclastic material (circa 50% with a dacitic or rhyolitic glass composition) has been erupted from the Mocho-Choshuenco complex during the last ca. 18 ka.

5.1. Eruptive frequency and scale

The estimated magnitude and age of the 27 identified units is summarised in Fig. 8. The large eruptions are not evenly spaced in time. The three Plinian events all occurred between 12.4 and 8.0 cal. ka BP (maximum modelled range). The most recent large (magnitude >5) event, Enco (MC15), occurred 1.5–1.7 cal. ka BP. Between Enco and Huilo (MC9), the youngest of the Plinian eruptions, deposits from only a few minor eruptions from the main edifice are preserved on the volcano flanks (MC11, MC12 and MC13), with the oldest estimated to have occurred 3.5–2.3 cal. ka BP. Between ca. 3.5 ka and ca. 8 ka (Huilo), the

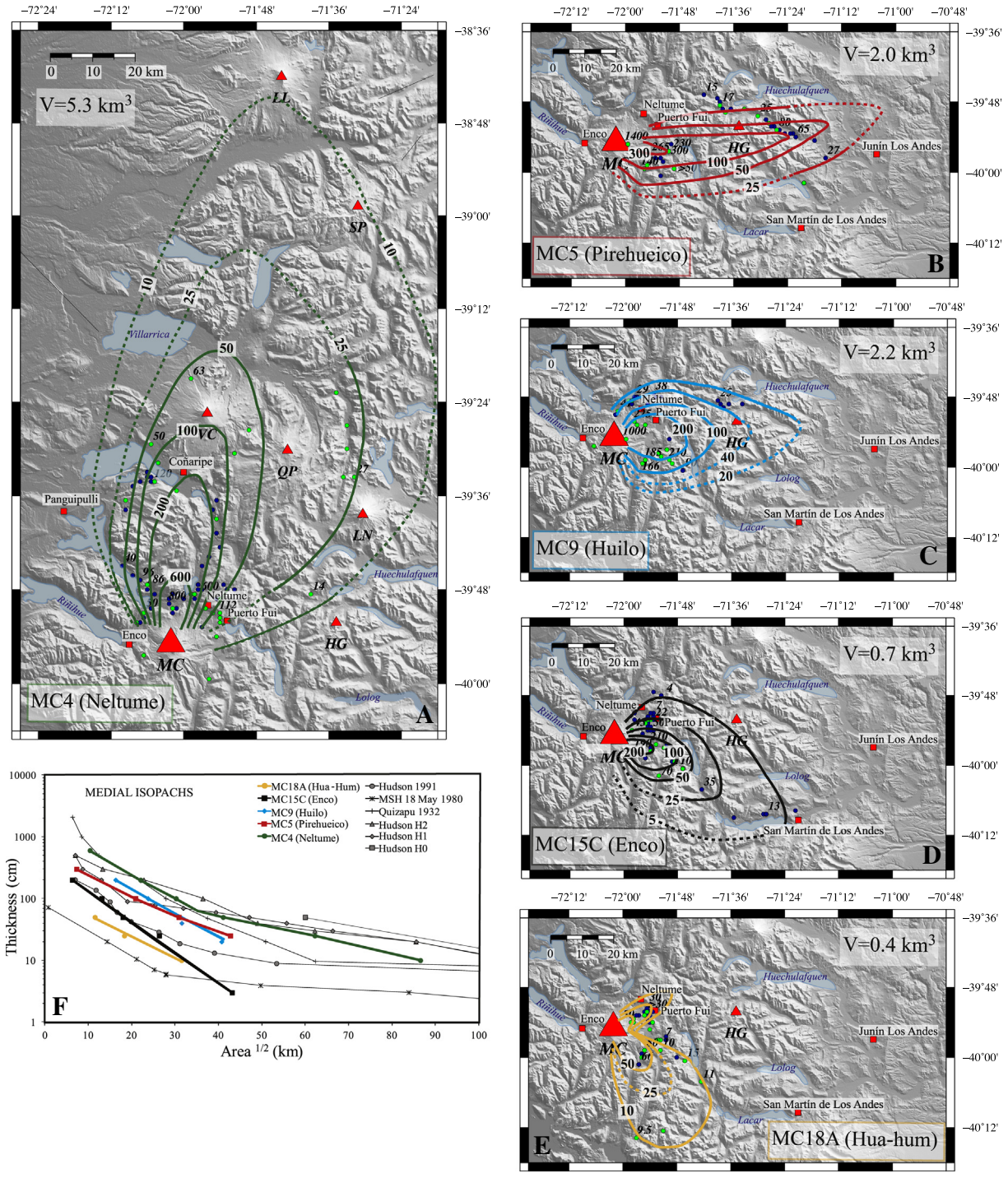

Fig. 7. Isopach maps (cm) for the five largest fall deposits from Mocho-Choshuenco. The volumes (V; bulk rock) and unit names are shown on the figure. Dashed lines are used instead of solid lines when there is greater uncertainty due to an absence of data. Localities, where the deposits are found, are marked with circles; selected sites have their corresponding thickness (cm) annotated. Green circles are sites where the deposit was additionally confirmed with glass and/or Fe–Ti oxide chemistry and dark-blue circles are sites where just field observations and stratigraphic position is used. Red triangles mark the regional volcanoes: MC = Mocho-Choshuenco, VC = Villarrica, QP = Quetrupillán, LN = Lanín, SP = Sollipulli, LL = LLaima and HG = Huanquihue Group. The towns and villages are labelled and marked with red squares. Graph F shows how the log(thickness) vs. area$^{1/2}$ varies between the different deposits from Mocho-Choshuenco and compared to those estimated from Volcán Hudson (Scasso et al., 1994; Naranjo and Stern, 1998; Weller et al., 2014), Quizapu (Hildreth and Drake, 1992) and Mount St Helens, USA (MSH; Sarna-Wojcicki et al., 1981). (For interpretation of the references to colour in this figure legend, the reader is referred to the web version of this article.)

only tephra units that are preserved are the minor scoria fall deposits of the Grupo Fui Tephra (8 sub-units MC10A–H, i.e., 8 eruptions). Most of these deposits are likely to originate from one of the many cones on the flanks inferred from their limited dispersal, proximity to the Fui cones and mafic composition. The geological record therefore suggests that there was a relatively long period (ca. >4.5 ka) of low explosivity from the central vent, apart from possible effusive activity. In contrast, we identify 11 tephra units, including the sub-Plinian Hua-Hum (MC18), eruption that are younger than Enco. This implies an increase in explosive frequency from the central volcano (one eruption every ~150 years compared to one every ~550 years prior to the Enco eruption, when the monogenetic cone eruptions are not considered). Given the limited dispersal of deposits associated with the monogenetic cones it is not yet possible to integrate these eruptions within the tephrostratigraphy

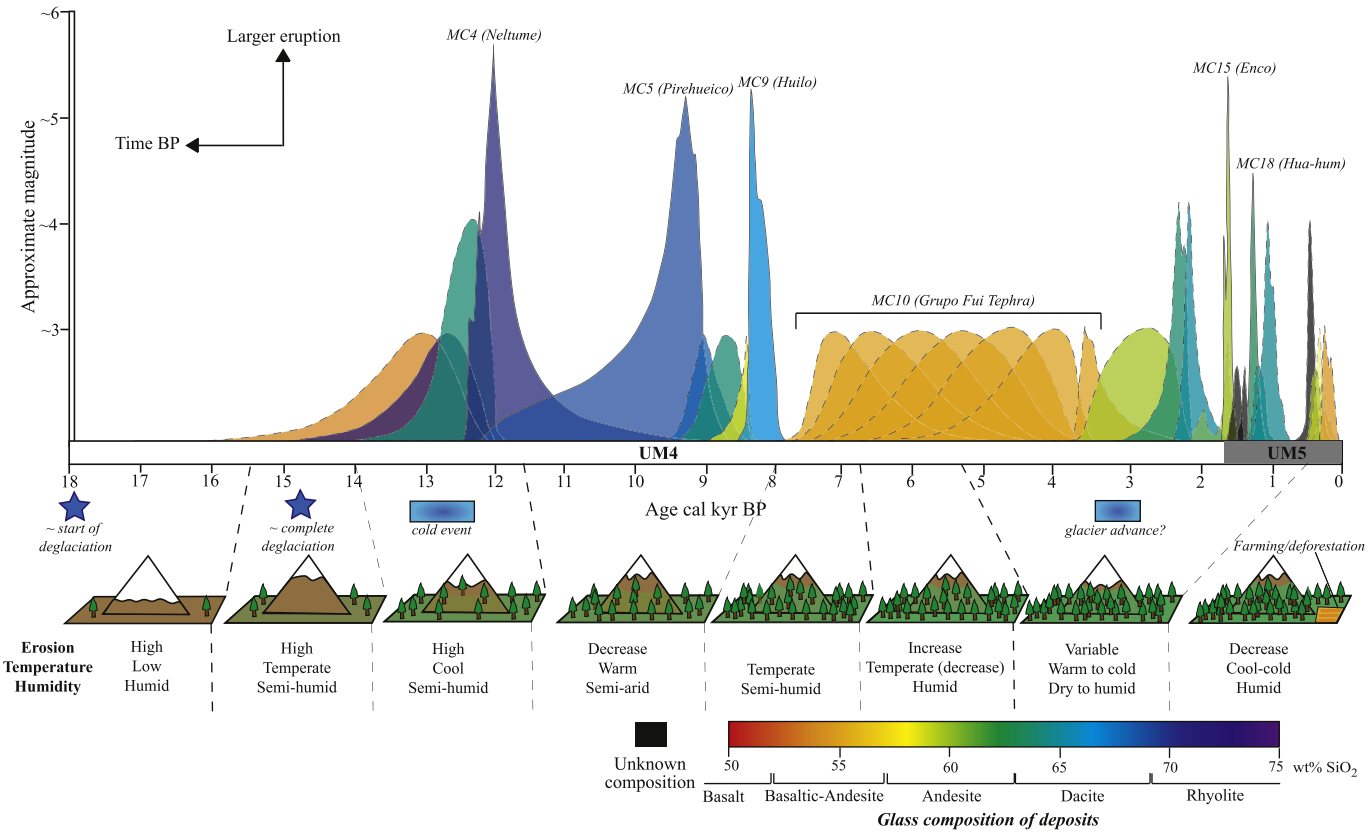

Fig. 8. Summary of the explosive history from Mocho-Choshuenco since deglaciation (~18 ka). Each unit is represented by its age probability distribution determined using Bayesian analysis of radiocarbon data, the height corresponds to the approximate magnitude (dashed lines used where magnitude is not well constrained) and the colour corresponds to the average SiO_2 glass composition. Magnitude = $\log_{10}$[eruption mass (kg) − 7] (Pyle, 2000). The erosion rates, temperature, humidity, climate and vegetation densities are inferred from the interpretations made on the Lago Puyehue core (ca. 90 km south of Mocho-Choshuenco; Bertrand et al., 2008; Vargas-Ramirez et al., 2008). (For interpretation of the references to colour in this figure legend, the reader is referred to the web version of this article.)

established for the more explosive eruptions. Thus, the tempo of the monogentic volcanism cannot be constrained.

The apparent temporal variations in central vent eruption frequency and size could reflect changes in the volcanic system or, instead, it may simply be an artefact of preservation due to variations in the regional climate. Pollen and sedimentological studies in Lago Puyehue and Los Mallines peat bog (both ca. 90 km south of Mocho-Choshuenco; Bertrand et al., 2008; Vargas-Ramirez et al., 2008) indicate that the temperature, humidity and vegetation density have varied since deglaciation began (ca. 18 ka; Fig. 8). Between 17.4 ka and 15.5 cal. ka BP low pollen concentrations and low carbon contents are found in the Lago Puyehue core (Vargas-Ramirez et al., 2008) suggesting sparse vegetation cover, and presumably poor soil development. This is an unfavourable environment for tephra preservation (e.g., Fontijn et al., 2014, for further discussion) and could explain why no deposits are found from this period. Between 5.3 ka and 0.52 cal. ka BP the peat core suggests that the climate was highly variable with both warm pulses (e.g., 4.6–4.3 cal. ka BP) and cold-humid periods (e.g., 3.4–2.9 cal. ka BP) recorded. The ca. 3 ka cold–humid period is linked to glacial advances in the central Andes (e.g., Bertrand et al., 2008). One implication of this is that proximal deposits on the flanks may have been eroded by advancing glaciers, removing evidence for older, smaller central vent events (e.g., sub-Plinian, magnitude ~<4) from the geological record. This could also explain the apparent low explosivity from the central vent between ca. 8–3.5 cal. ka BP where only the lower altitude cone forming eruptions (MC10 Grupo Fui Tephra) are preserved. Consequently, despite the high-resolution stratigraphy, we may still significantly underestimate eruption frequency, particularly for the activity pre-dating the most recent glacier advance (>ca. 2.9 cal. ka BP). We suggest that only central vent eruptions with a magnitude >4, or with a narrow dispersion (and magnitude >3), are expected to be preserved prior to the last glacier advance. Hence the more recent activity (<2.9 ka) is a truer reflection of the eruption behaviour at Mocho-Choshuenco.

Although changes in preservation might account for the apparent heightened eruption frequency in recent times it cannot explain the temporal spacing of the largest, magnitude >5, events. The three Plinian eruptions all occurred early in the post-glacial period over a relatively short period of time (12.4–8 cal. ka BP). Since Huilo (MC9), the last of the Plinian eruptions, Enco (MC15) is the only magnitude >5 eruption preserved. If there had been younger Plinian eruptions (or magnitude >5 events) they would have been detected. Therefore the geological record implies that there has been a change in eruption behaviour through time, with large eruptions more prevalent prior to 8 cal. ka BP. This may reflect a change in the magmatic system, perhaps as a response to changes in regional ice cover during deglaciation (e.g., Watt et al., 2013b), or to long-term fluctuations in magma supply rates and storage timescales.

Sixty volcanic centres in the SVZ have been active since the last glacial period. However, the published literature suggests only seven volcanoes have had more than 10 eruptions: Nevados de Chillán (12 eruptions), Lonquimay (23), Llaima (11), Villarica (23), Puyehue-Cordón Caulle (15), Calbuco (28) and Hudson (17) (references within Fontijn et al., 2014). At the majority of the volcanic centres (n = 36) only one to three post-glacial events are indentified. Our study shows that Mocho-Choshuenco has had at least 34 eruptions (with magnitude >~3; prior work only identified 4 eruptions) and therefore indicates that

it is one of the most active volcanoes in the SVZ. However many volcanoes in the SVZ have an incomplete record as they are still poorly studied or difficult to access. Around Mocho-Choshuenco there is a recently expanded road network (and hence outcrops) enabling easy access to the summit and flanks (east, north and west side). However, at other volcanoes the infrastructure is not as well developed, for example, at Volcán Hudson the nearest road is 30 km from the summit. Therefore finding any evidence of smaller past eruptions (magnitude <5) is highly challenging and consequently many studies focus solely on the largest, widespread events (e.g., Naranjo and Stern, 1998). Furthermore the high number of active volcanoes in the SVZ (60 volcanic centres) means many are still poorly studied (or the work has not yet been published in easily accessible or international literature). Therefore, presently, it is difficult to compare the explosive activity and eruptive frequency estimated for Mocho-Choshuenco to other volcanoes in the region with much certainty.

Only 18 volcanoes within the SVZ since the last glacial maximum have known deposits from a large eruption (magnitude >5; Fontijn et al., 2014), of which just nine, including Mocho-Choshuenco, have had multiple large events according to the published literature (Llaima, Villarrica, Puyehue-Cordón Caulle, Antillanca, Calbuco, Minchinmávida, Chaitén and Hudson). Further large eruptions have been identified but with insufficient published details to critically evaluate eruption parameters (e.g., Naranjo et al., 2001; Fierstein et al., 2013). Hudson is the only other volcano where more than two large units are recognised; H0, H1, H2 and H3, all of which have Plinian deposits (Naranjo and Stern, 1998; Weller et al., 2014). Plinian eruptions with volumes >1 km^3 are rare in the SVZ (23 eruptions, including this work, are identified in the published literature; references within Fontijn et al., 2014), with only Hudson, Chaitén, Calbuco, Mocho-Choshuenco and Puyehue-Cordón Caulle known to have more than one large fall deposit. Three large Plinian eruptions are identified from Mocho-Choshuenco (MC4 (Neltume), MC5 (Pirehueico) and MC9 (Huilo)), all of which have a dacitic melt composition. Therefore Mocho-Choshuenco is unusual in the SVZ in having evidence of four large eruptions, three of which generated by sustained Plinian eruption columns; hence it is potentially one of the most hazardous volcanoes in SVZ in terms of explosivity.

5.2. Regional tephra markers

Most deposits from Mocho-Choshuenco are dispersed to the north and east (due to prevailing wind directions, Fig. 7). Only two units are found in terrestrial sequences interbedded with deposits from neighbouring volcanoes: Neltume (MC4) and Hua-Hum (MC18). Hence Pirehueico (MC5), Huilo (MC9) and Enco (MC15), the other large and widely dispersed eruptions, are not useful regional markers, probably as their dispersion directions are roughly perpendicular to the volcanic arc. Neltume, the largest preserved deposits from an explosive eruption from Mocho-Choshuenco, has a NNE dispersion, which is uncommon in this region. Cha1, from Chaitén, is the only other Plinian eruption known to have a NNE dispersal in the SVZ (Watt et al., 2013a; Fontijn et al., 2014); the majority are dispersed east, ENE or ESE. Neltume deposits are confirmed, with chemistry, at more than nine outcrops (north of Lago Calafquén), interbedded with tephra deposits from the Villarrica–Quetrupillán–Lanín chain. The reconstructed isopach map (Fig. 7A) suggests that deposits could originally have been deposited around Sollipulli and Llaima too. Hence this unit is an invaluable regional marker.

Hua-Hum (MC18), a smaller and younger deposit than Neltume (MC4), is dispersed to the north-east and south-east. To the south-east, the larger lobe, deposits are found interbedded with deposits from Puyehue-Cordón Caulle (e.g., CLD153, 40°14′S 71°57′W). Unfortunately it has not been possible to assign the Puyehue-Cordón Caulle deposits to known events or correlate to the Puyehue-Cordón Caulle deposit interbedded with deposits from MC10 (Grupo Fui Tephra; Fig. 3J) and hence gain further stratigraphic constraints. They are inferred to come from Puyehue-Cordón Caulle as the glass chemistry of the deposits does not correlate to any proximal Mocho-Choshuenco deposit, it lies off the Mocho-Choshuenco compositional trend (particularly for K_2O vs. SiO_2; Supplementary material) and the glass has a rhyolitic composition similar to that of the Puyehue-Cordón Caulle 2011 eruption (Bertrand et al., 2014). No other rhyolite producing volcano has known eruptions that are likely to have deposits preserved near Puyehue-Cordón Caulle or Mocho-Choshuenco.

Although deposits from Mocho-Choshuenco are found interbedded around the Villarrica–Quetrupillán–Lanín chain there are only three localities around Mocho-Choshuenco where deposits from other volcanoes are observed; CLD153 (40°14′S 71°57′W), 115-03 (Fig. 3J) and 130112-3 (40°13′S 71°51′W). All three of these localities lie to the south of the edifice and preserve deposits from Puyehue-Cordón Caulle. This result illustrates two important features of the SVZ, which restricts the number of potential regional tephra marker beds. Firstly, the wind direction is predominantly to the east and consequently most volcanic eruptions in Chile get blown perpendicular to the volcanic arc and into Argentina. Secondly, only large eruptions (i.e., magnitude ≥5) are likely to be preserved at neighbouring volcanoes due to the typical wide spacing (>60 km) of volcanoes along the arc. This scale of eruption is uncommon in Chile (see Section 5.1 and Fontijn et al., 2014). Therefore in the SVZ it is rare to find interbedded tephra deposits from more than one volcanic centre preserved in terrestrial sites. On the other hand, preservation of the tephra in lake sediments is significantly better as they are not eroded or weathered in the same way that land deposits are. Consequently lakes in the region form excellent repositories for finer material (from smaller or more distal eruptions) and hence there is a greater potential for finding deposits from more than one volcano in lake cores. However, interpretations may be complicated by the delivery of tephra from run-off, rather than fallout, and from tectonic disturbances (e.g., Juvigné et al., 2008; Van Daele et al., 2014; Bertrand et al., 2014; Moernaut et al., 2014; Van Daele et al., 2015). Since the post-glacial tephra deposits from Mocho-Choshuenco now have well constrained chemistry, dispersion and ages they could be invaluable markers in the regional lake cores, both in Chile and Argentina.

6. Conclusions

A detailed study of the post-glacial tephra deposits from Volcán Mocho-Choshuenco has enabled the explosive activity to be accurately reconstructed. This new tephrostratigraphy shows that Mocho-Choshuenco is the source of more than 34 explosive eruptions and ~40 smaller eruptions forming monogenetic cones during the last 18 ka; this is the highest number of post-glacial explosive eruptions identified from a single volcanic centre in the SVZ. Analysis indicates that the eruptive frequency at Mocho-Choshuenco is one moderate-large (magnitude ≥3) eruption every ~440 years. During the past 1.7 kyrs, radiocarbon dating of formation UM5 suggests an eruptive frequency of one explosive eruption every ~150 years. This may be a truer reflection of the eruption frequency at Mocho-Choshuenco. This is particularly important to consider as the last known eruption from Mocho-Choshuenco was in 1864. Mocho-Choshuenco is estimated to have erupted ≥20 km^3 of pyroclastic material (ca. 50% with a dacitic to rhyolitic glass composition) during the last 18 ka, making it one of the most productive and active volcanoes in the SVZ since deglaciation.

The large new compositional dataset and eruption chronology means that the major late Quaternary tephra deposits from Mocho-Choshuenco are now well characterised, and may be used as regional stratigraphic marker beds. The Neltume deposits, which have a rare NNE dispersion, are found interbedded with tephra deposits from the Villarrica–Quetrupillán–Lanín chain and are expected to be preserved around Sollipulli and Llaima (~140 km NNE of Mocho-Choshuenco),

which could be used to help constrain the eruption chronology at these volcanoes.

The success of using this multi-phase approach to unravel the complicated volcanic stratigraphy at Mocho-Choshuenco suggests that a similar approach at other SVZ volcanoes could prove worthwhile. This would enable robust comparisons of eruption style and frequency between different volcanic centres, and could be used for hazard assessments in the region.

Acknowledgements

This work was supported by the Natural Environment Research Council (NERC) project 'Tempo of post-glacial volcanism in southern Chile' (NE/I013210/1). Full data associated with this paper are available in the online supplementary datasets, and at DOI: 10.6084/m9.figshare.1360020. HR is further supported by grants from the Old Members Trust (University College, Oxford) and Santander Academic Travel Award. DMP and TAM are supported by and contribute to the NERC National Centre for Earth Observation, of which the Centre for the Observation and Modelling of Earthquakes, Volcanoes and Tectonics (COMET+) is a part. We are greatly appreciative to Stefan Lachowycz, José Barrientos, Monse Cascante, Rogelio Fuentealba, Leandro Iturra, Rebecca Neely and Antonio Vásquez for invaluable assistance in the field, Huilo-Huilo Biological Reserve, in particular Tania Altamirano, for enabling vital access to the reserve to carry out essential field work and Norman Charnley for his assistance with the EMP analyses. The work was supported by the NERC Radiocarbon Facility NRCF010001 (allocation number 1753.1013). We are grateful for all the support and advice given by the NERC Radiocarbon Facility and SUERC AMS laboratory in East Kilbride, UK, particularly Steve Moreton. We thank Margaret Mangan for editorial handling and Judy Fierstein and an anonymous reviewer for their constructive reviews that greatly improved the manuscript.

Appendix A. Supplementary data

Supplementary data to this article can be found online at http://dx.doi.org/10.1016/j.jvolgeores.2015.04.003.

References

Bacon, C.R., Hirschmann, M.M., 1988. Mg/Mn partitioning as a test for equilibrium between coexisting Fe–Ti oxides. Am. Mineral. 73 (1–2), 57–61.
Bernales, 1990. Toponimia de Valdivia, Temuco. Ediciones Universidad de la Frontera.
Bertrand, S., Charlet, F., Charlier, B., Renson, V., Fagel, N., 2008. Climate variability of southern Chile since the last glacial maximum: a continuous sedimentological record from Lago Puyehue (40°S). J. Paleolimnol. 39 (2), 179–195. http://dx.doi.org/10.1007/s10933-007-9117-y.
Bertrand, S., Daga, R., Bedert, R., Fontijn, K., 2014. Deposition of the 2011–2012 Cordón Caulle tephra (Chile, 40°S) in lake sediments: implications for tephrochronology and volcanology. J. Geophys. Res Earth Surf. 119, 2555–2573. http://dx.doi.org/10.1002/2014JF003321.
Blockley, S.P., Ramsey, C.B., Pyle, D.M., 2008. Improved age modelling and high-precision age estimates of late Quaternary tephras, for accurate palaeoclimate reconstruction. J. Volcanol. Geotherm. Res. 177 (1), 251–262. http://dx.doi.org/10.1016/j.jvolgeores.2007.10.015.
Bronk-Ramsey, C.B., 2009a. Bayesian analysis of radiocarbon dates. Radiocarbon 51 (1), 337–360.
Bronk-Ramsey, C.B., 2009b. Dealing with outliers and offsets in radiocarbon dating. Radiocarbon 51 (3), 1023–1045.
Carey, S., Sparks, R.S.J., 1986. Quantitative models of the fallout and dispersal of tephra from volcanic eruption columns. Bull. Volcanol. 48 (2–3), 109–125. http://dx.doi.org/10.1007/BF01046546.
Carmichael, I.S.E., Nicholls, J., 1967. Iron-titanium oxides and oxygen fugacities in volcanic rocks. J. Geophys. Res. 72 (18), 4665–4687. http://dx.doi.org/10.1029/JZ072i018p04665.
Cobeñas, G., Thouret, J.C., Bonadonna, C., Boivin, P., 2012. The c. 2030 yr BP Plinian eruption of El Misti volcano, Peru: eruption dynamics and hazard implications. J. Volcanol. Geotherm. Res. 241, 105–120. http://dx.doi.org/10.1016/j.jvolgeores.2012.06.006.
Daggitt, M.L., Mather, T.A., Pyle, D.M., Page, S., 2014. AshCalc—a new tool for the comparison of the exponential, power-law and Weibull models of tephra deposition. J. Appl. Volcanol. 3 (1), 7. http://dx.doi.org/10.1186/2191-5040-3-7.
Devine, J.D., Rutherford, M.J., Norton, G.E., Young, S.R., 2003. Magma storage region processes inferred from geochemistry of Fe–Ti oxides in andesitic magma, Soufriere Hills Volcano, Montserrat, WI. J. Petrol. 44 (8), 1375–1400. http://dx.doi.org/10.1093/petrology/44.8.1375.
Droop, G.T.R., 1987. A general equation for estimating Fe^{3+} concentrations in ferromagnesian silicates and oxides from microprobe analyses, using stoichiometric criteria. Mineral. Mag. 51 (361), 431–435.
Echegaray, J., 2004. Evolución geológica y geoquímica del Centro Volcánico Mocho-Choshuenco, Andes del Sur. (Master Thesis). Universidad de Chile, Chile.
Echegaray, J., Moreno, H., Lopez-Escobar, L., 1994. El Deposito de Pomez Pliniana del Grupo Volcanico Mocho-Choshuenco, Andes del Sur (40°S). 1. Congreso Geologico Chileno, Chile, pp. 269–272.
Fierstein, J., 2007. Explosive eruptive record in the Katmai region, Alaska Peninsula: an overview. Bull. Volcanol. 69 (5), 469–509. http://dx.doi.org/10.1007/s00445-006-0097-y.
Fierstein, J., Nathenson, M., 1992. Another look at the calculation of fallout tephra volumes. Bull. Volcanol. 54 (2), 156–167. http://dx.doi.org/10.1007/BF00278005.
Fierstein, J., Sruoga, P., Amigo, A., Elissondo., M., Rosas, M., 2013. Tephra in Argentina establishes postglacial eruptive history of Laguna del Maule volcanic field in Chile. IAVCEI 2013 Scientific Assembly (abstract 3A2_3F–O11, 23 July).
Fontijn, K., Lachowycz, S.M., Rawson, H., Pyle, D.M., Mather, T.A., Naranjo, J.A., Moreno, H., 2014. Late Quaternary tephrostratigraphy of southern Chile and Argentina. Quat. Sci. Rev. 89, 70–84. http://dx.doi.org/10.1016/j.quascirev.2014.02.007.
Froggatt, P.C., Rogers, G.M., 1990. Tephrostratigraphy of high-altitude peat bogs along the axial ranges, North Island, New Zealand. N. Z. J. Geol. Geophys. 33 (1), 111–124. http://dx.doi.org/10.1080/00288306.1990.10427577.
Ghiorso, M.S., Evans, B.W., 2008. Thermodynamics of rhombohedral oxide solid solutions and a revision of the Fe–Ti two-oxide geothermometer and oxygen-barometer. Am. J. Sci. 308 (9), 957–1039. http://dx.doi.org/10.2475/09.2008.01.
Glasser, N.F., Jansson, K.N., Harrison, S., Kleman, J., 2008. The glacial geomorphology and Pleistocene history of South America between 38°S and 56°S. Quat. Sci. Rev. 27 (3), 365–390. http://dx.doi.org/10.1016/j.quascirev.2007.11.011.
Hildreth, W., Drake, R.E., 1992. Volcán Quizapu, Chilean Andes. Bull. Volcanol. 54 (2), 93–125. http://dx.doi.org/10.1007/BF00278002.
Hogg, A.G., Hua, Q., Blackwell, P.G., Niu, M., Buck, C.E., Guilderson, T.P., Heaton, T.J., Palmer, J.G., Reimer, P.J., Reimer, R.W., Turney, C.S.M., Zimmerman, S.R., 2013. SHCal13 Southern Hemisphere calibration, 0–50,000 cal yr BP. Radiocarbon 55 (4), 1889–1903. http://dx.doi.org/10.2458/azu_js_rc.55.16783.
Hulton, N.R., Purves, R.S., McCulloch, R.D., Sugden, D.E., Bentley, M.J., 2002. The last glacial maximum and deglaciation in southern South America. Quat. Sci. Rev. 21 (1), 233–241. http://dx.doi.org/10.1016/S0277-3791(01)00103-2.
Jarosewich, E., Nelen, J.A., Norberg, J.A., 1980. Reference samples for electron microprobe analysis. Geostand. Newslett. 4 (1), 43–47. http://dx.doi.org/10.1111/j.1751-908X.1980.tb00273.x.
Jochum, K.P., Stoll, B., Herwig, K., Willbold, M., Hofmann, A.W., Amini, M., Aarburg, S., Abouchami, W., Hellebrand, E., Mocek, B., Raczek, I., Stracke, A., Alard, O., Bouman, C., Becker, S., Dücking, M., Brätz, H., Klemd, R., de Bruin, D., Canil, D., Cornell, D., de Hoog, C., Dalpé, C., Danyushevsky, L., Eisenhauer, A., Gao, Y., Snow, J.E., Groschopf, N., Günther, D., Latkoczy, C., Guillong, M., Hauri, E., Höfer, H.E., Lahaye, Y., Horz, K., Jacob, D.E., Kasemann, S.A., Kent, A.J.R., Ludwig, T., Zack, T., Mason, P.R.D., Meixner, A., Rosner, M., Misawa, K., Nash, B.P., Pfänder, J., Premo, W.R., Sun, W.D., Tiepolo, M., Vannucci, R., Vennemann, T., Wayne, D., Woodhead, J.D., 2006. MPI-DING reference glasses for in situ microanalysis: New reference values for element concentrations and isotope ratios. Geochem. Geophys. Geosyst. 7 (Q02008). http://dx.doi.org/10.1029/2005GC001060.
Juvigné, E., Bertrand, S., Heuschen, B., Tallier, E., 2008. Téphrostratigraphie de sediments lacustres situés en context géodynamique actif: exemple des sediments du lac Icalma (Chili, zone volcanique sud, 38°S). Quaternaire 19, 175–189. http://dx.doi.org/10.4000/quaternaire.3532.
Kaplan, M.R., Fogwill, C.J., Sugden, D.E., Hulton, N.R.J., Kubik, P.W., Freeman, S.P.H.T., 2008. Southern Patagonian glacial chronology for the Last Glacial period and implications for Southern Ocean climate. Quat. Sci. Rev. 27 (3), 284–294. http://dx.doi.org/10.1016/j.quascirev.2007.09.013.
Lowe, D.J., 1988. Stratigraphy, age, composition, and correlation of late Quaternary tephras interbedded with organic sediments in Waikato lakes, North Island, New Zealand. N. Z. J. Geol. Geophys. 31 (2), 125–165. http://dx.doi.org/10.1080/00288306.1988.10417765.
Lowe, D.J., 2011. Tephrochronology and its application: a review. Quat. Geochronol. 6 (2), 107–153. http://dx.doi.org/10.1016/j.quageo.2010.08.003.
Marcaida, M., Mangan, M.T., Vazquez, J.A., Bursik, M., Lidzbarski, M.I., 2014. Geochemical fingerprinting of Wilson Creek formation tephra layers (Mono Basin, California) using titanomagnetite compositions. J. Volcanol. Geotherm. Res. 273, 1–14. http://dx.doi.org/10.1016/j.jvolgeores.2013.12.008.
Moernaut, J., Daele, M.V., Heirman, K., Fontijn, K., Strasser, M., Pino, M., Urrutia, R., De Batist, M., 2014. Lacustrine turbidites as a tool for quantitative earthquake reconstruction: new evidence for a variable rupture mode in south central Chile. J. Geophys. Res. Solid Earth 119 (3), 1607–1633. http://dx.doi.org/10.1002/2013JB010738.
Moreno, H., Lara, L., 2007. Geologia del Complejo Volcánico Mocho-Choshuenco Carta Geológica de Chile. Serie Geología Básica 107, 1–27.
Moreno, H., and Naranjo, J.A. 2006. Peligros del Complejo Volcánico Mocho-Choshuenco, Región de los Lagos, escala 1:50.000. Servicio Nacional de Geología y Minería, Carta Geológica de Chile, Serie Geología Ambiental N° 9.
Naranjo, J.A., Stern, C.R., 1998. Holocene explosive activity of Hudson Volcano, southern Andes. Bull. Volcanol. 59 (4), 291–306. http://dx.doi.org/10.1007/s004450050193.
Naranjo, J.A., Polanco, E., Lara, L., Moreno, H., Stern, C.R., 2001. Holocene tephra-fall deposits of Southern and Austral Andes Volcanic Zones (33–54°S): eruption recurrence. Compt. Rendus Geosci. 52, 109 (abstract).

Newhall, C.G., Self, S., 1982. The Volcanic Explosivity Index (VEI) an estimate of explosive magnitude for historical volcanism. J. Geophys. Res. 87 (C2), 1231–1238. http://dx.doi.org/10.1029/JC087iC02p01231.
Pérez, S., 2005. Volcanismo Explosivo Postglacial del Complejo Volcánico Mocho-Choshuenco. (Master Thesis). Universidad de Concepción, Facultad de Ciencias Quimicas, Chile.
Pyle, D.M., 1989. The thickness, volume and grainsize of tephra fall deposits. Bull. Volcanol. 51 (1), 1–15. http://dx.doi.org/10.1007/BF01086757.
Pyle, D.M., 1995. Assessment of the minimum volume of tephra fall deposits. J. Volcanol. Geotherm. Res. 69 (3), 379–382. http://dx.doi.org/10.1016/0377-0273(95)00038-0.
Pyle, D.M., 2000. Sizes of volcanic eruptions. In: Sigurdsson, H. (Ed.), Encyclopedia of Volcanoes. 1. Academic Press, San Diego, pp. 263–269.
Sarna-Wojcicki, A.M., Shipley, S., Waitt Jr., R.B., Dzurisin, D., Wood, S.H., 1981. Areal distribution, thickness, mass, volume, and grain size of air-fall ash from the six major eruptions of 1980. In: Lipman, P.W., Mullineaux, D.R. (Eds.), The 1980 eruptions of Mount St Helens, Washington. USGS Prof Paper 1250, pp. 577–600.
Scasso, R.A., Corbella, H., Tiberi, P., 1994. Sedimentological analysis of the tephra from the 12–15 August 1991 eruption of Hudson volcano. Bull. Volcanol. 56 (2), 121–132. http://dx.doi.org/10.1007/BF00304107.
Scott, K.M., 1988. Origins, behavior, and sedimentology of lahars and lahar-runout flows in the Toutle–Cowlitz River system. U.S. Geol. Surv. Prof. Pap. 1447-A.
Sepulveda, M.E.P., 2004. La historia eruptiva de los volcanes hispanoamericanos (Siglos XV1 al XX): El model Chileno.
Shane, P., 1998. Correlation of rhyolitic pyroclastic eruptive units from the Taupo volcanic zone by Fe–Ti oxide compositional data. Bull. Volcanol. 60 (3), 224–238. http://dx.doi.org/10.1007/s004450050229.
Shane, P., 2000. Tephrochronology: a New Zealand case study. Earth Sci. Rev. 49 (1), 223–259. http://dx.doi.org/10.1016/S0012-8252(99)00058-6.
Shane, P., Smith, V.C., Nairn, I., 2003. Biotite composition as a tool for the identification of Quaternary tephra beds. Quat. Res. 59 (2), 262–270. http://dx.doi.org/10.1016/S0033-5894(03)00012-7.
Smith, V.C., Pearce, N.J., Matthews, N.E., Westgate, J.A., Petraglia, M.D., Haslam, M., Lane, C.S., Korisettar, R., Pal, J.N., 2011a. Geochemical fingerprinting of the widespread Toba tephra using biotite compositions. Quat. Int. 246 (1), 97–104. http://dx.doi.org/10.1016/j.quaint.2011.05.012.
Smith, V.C., Isaia, R., Pearce, N.J.G., 2011b. Tephrostratigraphy and glass compositions of post-15 kyr Campi Flegrei eruptions: implications for eruption history and chronostratigraphic markers. Quat. Sci. Rev. 30 (25–26), 3638–3660. http://dx.doi.org/10.1016/j.quascirev.2011.07.012.
Stern, C.R., 1991. Mid-Holocene tephra on Tierra del Fuego (54°S) derived from the Hudson volcano (46°S): evidence for a large explosive eruption. Andean Geol. 18 (2), 139–146. http://dx.doi.org/10.5027/andgeoV18n2-a04.
Van Daele, M., Moernaut, J., Silversmit, G., Schmidt, S., Fontijn, K., Heirman, K., Vandoorne, W., De Clercq, M., van Acker, J., Wolff, C., Pino, M., Urrutia, R., Robert, S.J., Vincze, L., De Batist, M., 2014. The 600 yr eruptive history of Villarrica Volcano (Chile) revealed by annually laminated lake sediments. Geol. Soc. Am. Bull. 126, 481–498. http://dx.doi.org/10.1130/B30798.1.
Van Daele, M., Moernaut, J., Doom, L., Boes, E., Fontijn, K., Heirman, K., Vandoorne, W., Hebbeln, D., Pino, M., Urrutia, R., Brümmer, R., De Batist, M., 2015. A comparison of the sedimentary records of the 1960 and 2010 great Chilean earthquakes in 17 lakes: implications for quantitative lacustrine palaeoseismology. Sedimentology http://dx.doi.org/10.1111/sed.12193.
Vargas-Ramirez, L., Roche, E., Gerrienne, P., Hooghiemstra, H., 2008. A pollen-based record of late glacial–Holocene climatic variability in the southern lake district, Chile. J. Paleolimnol. 39 (2), 197–217. http://dx.doi.org/10.1007/s10933-007-9115-0.
Venezky, D.Y., Rutherford, M.J., 1999. Petrology and Fe–Ti oxide reequilibration of the 1991 Mount Unzen mixed magma. J. Volcanol. Geotherm. Res. 89 (1), 213–230. http://dx.doi.org/10.1016/S0377-0273(98)00133-4.
Vidal Gormaz, F., 1869. Esploración del río Calle-Calle, provincia de Valdivia. XXXII. Anales de la Universidad de Chile, pp. 34–35.
Watt, S.F., Pyle, D.M., Naranjo, J.A., Rosqvist, G., Mella, M., Mather, T.A., Moreno, H., 2011. Holocene tephrochronology of the Hualaihue region (Andean southern volcanic zone, ~42°S), southern Chile. Quat. Int. 246 (1), 324–343. http://dx.doi.org/10.1016/j.quaint.2011.05.029.
Watt, S.F., Pyle, D.M., Mather, T.A., 2013a. Evidence of mid-to late-Holocene explosive rhyolitic eruptions from Chaitén Volcano, Chile. Andean Geol. 40 (2), 216–226. http://dx.doi.org/10.5027/andgeoV40n2-a02.
Watt, S.F., Pyle, D.M., Mather, T.A., 2013b. The volcanic response to deglaciation: Evidence from glaciated arcs and a reassessment of global eruption records. Earth Sci. Rev. 122, 77–102. http://dx.doi.org/10.1016/j.earscirev.2013.03.007.
Weller, D., Miranda, C.G., Moreno, P.I., Villa-Martínez, R., Stern, C.R., 2014. The large late-glacial Ho eruption of the Hudson volcano, southern Chile. Bull. Volcanol. 76 (6), 1–18. http://dx.doi.org/10.1007/s00445-014-0831-9.